Master of Science Thesis in Electrical Engineering
Department of Electrical Engineering, Linköping University, 2016

Physically Based Models for Predicting Exhaust Temperatures in SI Engines

Andrej Verem and Hiren Kerai

Master of Science Thesis in Electrical Engineering

Physically Based Models for Predicting Exhaust Temperatures in SI Engines

Andrej Verem and Hiren Kerai

LiTH-ISY-EX--16/4943--SE

Supervisor: **Xavier Llamas Comellas**
ISY, Linköpings universitet
Martin Larsson
Volvo Cars

Examiner: **Lars Eriksson**
ISY, Linköpings universitet

Division of Vehicular Systems
Department of Electrical Engineering
Linköping University
SE-581 83 Linköping, Sweden

Abstract

To have knowledge about the gas and material temperatures in the exhaust system of today's vehicles is of great importance. These temperatures need to be known for component protection, control- and diagnostic purposes. Today mostly map-based models are used which are not accurate enough and difficult to tune since it consist of many parameters.

In this thesis physically based models are developed for several components in the exhaust system. The models are derived through energy balances and are more intuitive compared to the current map-based models. The developed models are parameterized and validated with measurements from wind tunnel experiments and driving scenarios on an outdoor track.

The engine out model is modeled theoretically and is therefore not parameterized or validated. The model for the temperature drop over the exhaust manifold could not be validated due to the pulsations occurring in the exhaust manifold, however suggestions on how to solve this problem are given in this report. The models for the turbocharger, the catalyst and the downpipe are parameterized and validated with good results in this thesis. The mean absolute error for the validation data set for the turbocharger is 0.46 % and 1.01 % for the catalyst. The mean absolute percentage error for the downpipe is 1.07 %.

Acknowledgments

We would like to thank Volvo Cars for giving us the opportunity to write this thesis. We would also like to thank Anders Boteus and everyone on our division for assisting us with our work and providing us with information. Specially we would like to thank our supervisor, Martin Larsson at Volvo Cars for all the countless hours of help. Without you this thesis would not be possible. Furthermore, we would also like to thank our supervisor at Linköping University, Xavier Llamas Comellas for answering our questions and for the great input on the report. We would also like to thank Fredrik Wemmert for his expertise and his ideas which has been valuable for this thesis. Further, a big thanks to Reine Olsson which has helped us in the workshop with our extensive measurement setup. Finally we would like to thank Professor Lars Eriksson for making this thesis a reality. His enthusiasm for teaching has given us much knowledge in the field of engine control and his work has been important for this thesis.

Göteborg, June 2016
Andrej and Hiren

Contents

Notation

Abbreviations

Abbreviation	Description
BSR	Blade Speed Ratio
ECM	Engine Control Module
IVC	Inlet Valve Closing
MAPE	Mean Absolute Percentage Error
PDE	Partial Differential Equation
TDC	Top Dead Centre
TWC	Three-Way Catalyst

1 Introduction

In todays exhaust system for production petrol engines no temperatures are measured by sensors, even though several exhaust temperatures are required by the control systems for protection, control and for diagnostic purposes. Instead the exhaust temperatures are estimated by map-based models. These models are hard to understand and calibrate.

However, in recent years the accuracy of these models have been questioned, primarily due to stricter diagnostic requirements. Therefore, new models with higher accuracy to estimate these temperatures are sought for.

1.1 Problem Formulation

The expectations from Volvo Cars Corporation are to acquire temperature models which are simple enough to be implemented in the control system but advanced enough to obtain sufficient accuracy. The goal of this master thesis is to develop physically based temperature models for different parts of the exhaust system of a petrol engine. The main goal with the physically based models is that they can be reused on different engine configurations.

The aim with these developed models is that they will give more accurate prediction which will improve control and diagnostics performance and replace the current map-based models. Moreover, the proposed models should be able to reduce the amount of required measurements for parameterization, compared to the current requirements for the map-based models.

1.2 Purpose and Goal

The modeled temperatures will be used for component protection, engine control and diagnostic purposes.

Primarily there are five temperatures which are to be estimated, these models are marked in Figure 1.1. The models are listed below.

- The temperature of the exhaust gas after the exhaust valve directly after opening ($T_{ENG,OUT}$).
- The temperature of exhaust gas before the turbo ($T_{BE,TURB}$).
- The temperature of exhaust gas after the turbo ($T_{AF,TURB}$).
- The temperature 25 mm into the first catalyst brick ($T_{CAT1,25}$).
- The temperature before the muffler ($T_{BE,MUFF}$).

The engine out temperature will only be modeled theoretically. The theoretical approach will consist of the describing equations but no parameterization and validation will be performed.

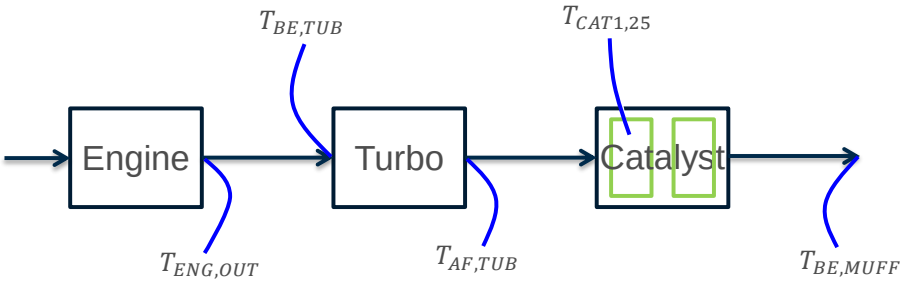

Figure 1.1: *Diagram of the temperatures to be modeled.*

1.3 Related Research

This section describes the related research performed in the field.

1.3.1 Cylinder-Out Temperature

The gas temperature out from the cylinders is crucial when it comes to modeling the inlet temperature to the turbocharger and the catalyst. In [10] an analytic cylinder pressure model is developed and validated. The method used in the paper is based on parameterization of an Otto cycle where variations in spark advance and air-to-fuel ratio are included. This paper is used as inspiration for the modeling of the cylinder-out temperature since the pressure change in the cylinder is important when modeling this temperature. Like the previous paper, similar work is made in [8]. A model for the temperature at the exhaust valve is

derived in [2]. It is based on the in-cylinder pressure which is built upon parameterization of the ideal Otto cycle, similar to [10]. Similar work is made in [18] where an analysis of the in-cylinder temperature is performed. Different residual gas fraction models are found in [15] and [26]. Through this project both the suggested one in [26] and in [15] is used. Further on another cylinder-out model is derived in [13]. Most equations where gathered from [14] to model the cylinder-out temperature in this thesis. This paper and the work in this master thesis is similar to the work done in [2].

In [6] the temperature at the exhaust port is obtained using the first law of thermodynamics. The exhaust port temperature is divided into multiple control volumes where heat losses are included. In addition to this, two in-cylinder heat transfer models are suggested in [19]. The first model is based on assumptions of incompressible flows and the second one is a model with full variable density effects. In [3] cylinder temperature models are derived and used to investigate the connection between the temperature and ionization currents. Both single-zone and two-zone models are suggested. Furthermore it is also assumed that the models are zero-dimensional. Similar to this paper a single-zone model was used in this project to compute the temperature in the cylinder.

1.3.2 Temperature before the Turbocharger

Concerning the modeling of the temperature drop between the cylinders and the turbocharger three different models has been developed and validated in [9]. The models in the paper does not explicitly model the dual wall of the manifold, but they seem to manage it very well according to the author. Inspiration is gathered from this paper since heat losses into the engine block is considered which is implied in the paper. The models derived in [12] does however treat a dual wall exhaust manifold. Furthermore [12] focuses more on proving that the dual wall exhaust manifold conserves more heat. In [23] exhaust manifolds with different shapes are treated. Steady state models are derived for the different exhaust systems configurations. Another approach of modeling the exhaust manifold heat transfer is found in [25]. Similar to other research, this one is based on a straightforward energy balance. In [4] an extensive overview of the heat transfer is given with resistor-capacitor thermal networks. The derived models are suitable both for steady state and transient simulations. Most inspiration for the exhaust manifold model is gathered from [22] combined with [9].

1.3.3 Temperature after the Turbocharger

A one dimensional non-adiabatic heat transfer model over the turbocharger is developed and validated in [21]. In [1] an investigation of the heat transfer from a turbocharger is performed. The authors state that the heat transfer from the turbocharger is dependent on the inlet temperature, the velocity of the exhaust gas and the ambient temperature. Moreover, their experiments show that the temperature depends on the previous load point when transient load steps are made. According to them, the temperature of the working fluids depends on the wall temperature of the turbocharger. An attempt to simulate the heat losses from

the turbine is done in [24]. Through measurements of the heat transfer it is shown that the major heat transfer is due to convection and radiation. A smaller amount of heat losses occurs due to heat transfer to the cooling water and the lubrication oil. In [17] a turbocharger model including heat transfers is developed for control purposes. The paper explains the model as well as an overview of curve fitting techniques. The approach taken in this thesis is inspired from [22] for the heat loss to the body housing and the gas expansion is described by a method from [17] and [14].

1.3.4 Temperatures in the Catalyst and after the Catalyst

A control oriented model for the three-way catalyst has been derived from physical partial differential equations (PDE) in [22]. The paper describes how the PDE's are derived and simplified. It also shows how the measurement sensors are placed and refers to other interesting papers with more thorough information about catalyst temperature modeling. However, this model does not take into account for all different specific chemical reactions in the catalyst. A lumped term is used instead to make the model fit for online usage. A similar model as in [22] is presented in [5], the big difference between these is that [5] takes the chemical reactions in the catalyst into consideration. Moreover, information about chemical modeling and exothermic reactions is found in [20], where the 15 most important chemical reaction formulas are listed as well as their heat release. However, for this thesis the approach taken in [22] is used with some minor modifications. The model used for the downpipe is also inspired from the same paper.

1.4 Outline

The report consists of five chapters, the structure is

- Introduction
- Measurements
- Models
- Results and Discussion
- Conclusions

The introduction discusses the background of the problem, the purpose and the goal of the thesis as well as the literature study. In the following chapter the measurements are discussed as well as sensor placement. The next chapter treats the modeling, containing all from theory to complete models. In the results section the model simulation together with the model validation are presented along with calibration values and relative errors of each model. The last section of the thesis contains the conclusion of the thesis work and the potential future work.

2
Measurements

To develop physically based models, measurement data is needed. The data is needed for calibration, validation and to build knowledge about the systems behavior. This chapter contains the description about the measurements, required measurement setup and analysis of the data.

2.1 Preparations for the Measurements

This section describes how the vehicle used for the measurements was prepared to be able to perform the desired measurements.

2.1.1 Exhaust Manifold

The exhaust manifold that is used in the equipped car is a dual wall manifold. To be able to capture the main temperature changes it is necessary to install an extensive setup of thermocouples. The first wall layer consists of four pipes from each cylinder that connects in a small volume before the turbocharger. These four pipes are covered with a second metallic layer and lastly there is an isolation cover on the outer side. The construction of the exhaust manifold is represented in Figures 2.1 and 2.2. To be able to estimate heat transfer coefficients it is necessary to measure the temperature on each layer and at the same time measure the gas temperature and the surrounding temperature.

Figure 2.1: *3D model of the exhaust manifold. Shows how the exhaust manifold is built of multiple layers.*

Figure 2.2: *3D model of the runner's shape.*

The measurements on the exhaust manifold consist of five different levels which are shown in Figure 2.3 and 2.4. The first level is inside the pipes, measuring the inner gas temperature. The material temperature of the inner and outer wall, the surface of the isolation layer and the surrounding temperature are measured. Different thermocouples sizes are used since it is not possible to measure with thin thermocouples in the high temperature. Thin thermocouples can easily be destroyed if exposed to too high temperatures. When measuring the inner gas temperatures, thermocouples with a diameter of 3 mm are used. The same type of sensor is also used for measuring the material temperature of the first layer. However, the temperatures of the outer layer as well as the isolation layer are measured with attached surface thermocouples. The surface sensors are welded on the outer wall layer. The isolation layer consists of aluminium and the sensors are pasted on with heat resistant glue since welding is not possible.

The surrounding temperature is measured through mounted sensors at 15 to 25 cm from the outermost layer. It is impossible to measure the temperature correctly since the measured temperature is a mean value temperature of surrounding objects. Furthermore, the exhaust gas temperature gets influenced by radiation from the walls. The ambient temperature close to the exhaust manifold is measured with and without a radiation protection to see how it influence the temperature reading. An overview of the different thermocouples position is shown in Figure 2.3

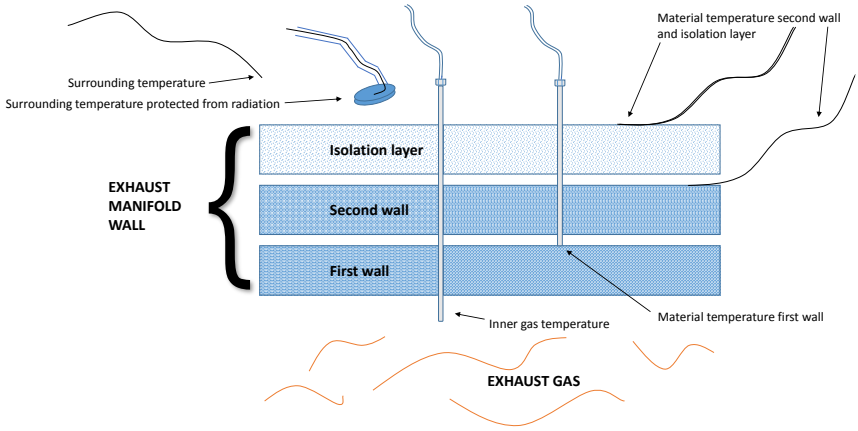

Figure 2.3: *Diagram about the different temperature measurement points on the exhaust manifold.*

The setup of Figure 2.3 is built in the same manner on five different places. In Figure 2.4 the numbers 1, 2, 3, 5 and 7 represent different points where exhaust gas temperature, material temperature on the inner and the outer walls are measured. At number 4 the exhaust gas temperature between the walls as well as the material temperature of the outer wall is measured. At 6 the material temperature of the outer wall and the exhaust gas temperature are measured. Finally the material temperatures of the flanges are measured in 8 and 9.

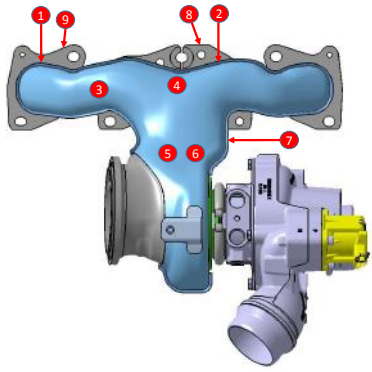

Figure 2.4: *Sensor placement diagram on the exhaust manifold.*

Table 2.1: *Thermocouples at exhaust manifold.*

Measuring location	Number in Figure 2.4
Air temperature near outer layer	(-)
Air temperature near outer layer with radiation protection	(-)
Gas temperature	(1)
Material temperature of wall 1	(1)
Material temperature of wall 2	(1)
Gas temperature	(2)
Material temperature of wall 1	(2)
Material temperature of wall 2	(2)
Gas temperature	(3)
Material temperature of wall 1	(3)
Material temperature of wall 2	(3)
Gas temperature between wall 1 and wall 2	(4)
Material temperature of wall 2	(4)
Gas temperature	(5)
Material temperature of wall 1	(5)
Material temperature of wall 2	(5)
Gas temperature	(6)
Material temperature of wall 2	(6)
Gas temperature	(7)
Material temperature of wall 1	(7)
Material temperature of wall 2	(7)
Material temperature of flange	(8)
Material temperature of flange	(9)

2.1.2 Turbocharger

In order to capture the heat losses in the turbocharger it is necessary to obtain knowledge about the temperature drop due to the gas expansion happening in the turbine. This information can be gathered through a speed sensor together with pressure sensors before and after the turbine. To model the temperature drop the exhaust gas temperatures before and after the turbine are essential. The exhaust gas temperature before the turbine is obtained from the exhaust manifold measurements, number 5 and 6 in Table 2.1 and Figure 2.4. The sensors mounted on the turbocharger are shown in Figure 2.5.

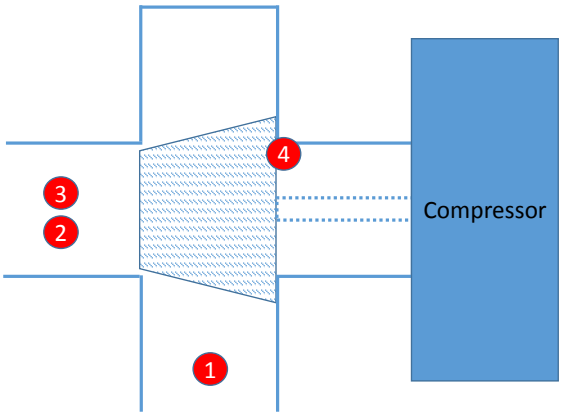

Figure 2.5: *Diagram about the different measurement points on the turbocharger .*

Table 2.2: *Thermocouples at turbocharger.*

Measuring location	Number in Figure 2.5
Pressure before turbocharger	(1)
Pressure after turbocharger	(2)
Temperature gas after turbocharger	(3)
Turbine speed sensor	(4)

2.1.3 Catalyst

The catalytic converter in the vehicle is prepared with a total of seven gas temperature sensors and 9 surface temperature sensors. The first gas temperature is placed right before the first brick inside the catalyst, which is denoted with number 1 in Figure 2.6. Two gas temperature sensors are mounted in the first catalyst brick, where the first sensor is placed 25 mm into the brick and the second sensor 50 mm into the brick, these are denoted 2 and 3 in the Figure. In addition to that one gas temperature sensor is placed after the first brick (number 4). Furthermore, two thermocouples are placed into the second brick, where the first is placed 25 mm into the brick and the second one 55 mm in, these are presented by number 5 and 6 in the Figure. One last thermocouple for gas temperature is placed after the second catalyst brick (number 7 in the Figure). The placement is planned in such a way that as much information as possible is gathered about the effects of the exothermic reactions taking place in the catalyst.

The sensors for the surface temperatures are placed as close to the gas temperature sensors as possible. This is done to get a good understanding of how much energy flows out of the catalyst to the surroundings. Some parts of the catalyst are equipped with a second isolation layer. At those places the temperature of

both the inner and outer surface are measured.

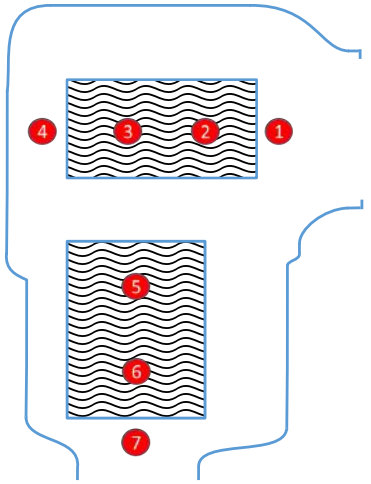

Figure 2.6: *Diagram about the different measurement points on the catalyst. At these points the gas temperature as well as the surface temperatures are measured.*

Table 2.3: *Thermocouples at catalyst.*

Measuring location	Number in Figure 2.6
Temperature gas before catalyst	(1)
Surface temperature for first layer	(1)
Surface temperature for second layer	(1)
Temperature gas/material 25 mm in brick 1	(2)
Surface temperature for first layer	(2)
Temperature gas/material 50 mm in brick 1	(3)
Surface temperature for first layer	(3)
Surface temperature for second layer	(3)
Temperature gas after brick 1	(4)
Surface temperature for first layer	(4)
Temperature gas/material 25 mm in brick 2	(5)
Surface temperature for first layer	(5)
Temperature gas/material 55 mm in brick 2	(6)
Surface temperature for first layer	(6)
Temperature gas after catalyst	(7)
Surface temperature for first layer	(7)

2.1.4 Downpipe

The downpipe is constructed of a metal net wrapped around a folded pipe which is connected to the catalyst. A picture of the downpipe is shown in Figure 2.7. During a driving operation the exhaust system is exposed to stress and ruptures

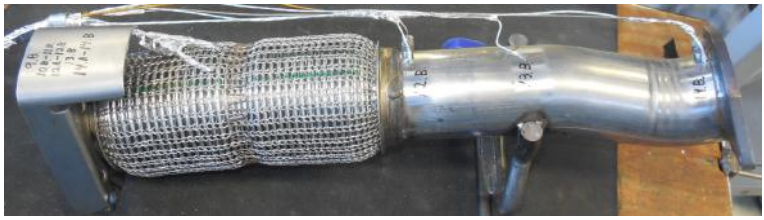

Figure 2.7: *Picture of the downpipe.*

that can occur due to the stiffness of the exhaust pipes. With the help of the downpipe this stress is decreased and it allows the exhaust system to move and become more flexible. Due to the construction it is not possible to mount a gas temperature sensor on the flexible part of the pipe, however three surface temperature sensors are mounted on this part. The connecting pipe after the flex pipe is equipped with gas temperature sensors in the beginning and in the end of the pipe. In addition to that three more surface temperature sensors are mounted in order to measure the material temperature. The placement of the sensors are shown in Figure 2.8 and described in Table 2.4.

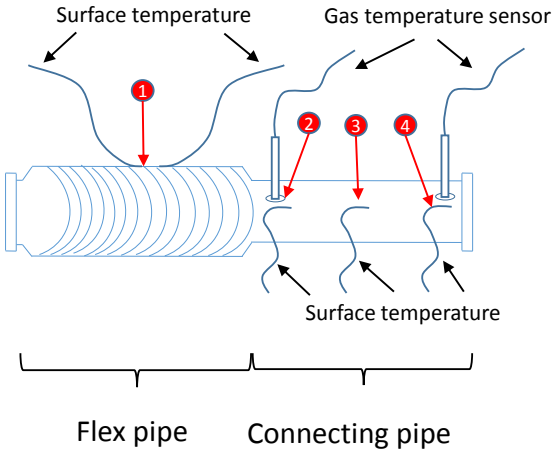

Figure 2.8: *Diagram about the different temperatures that are measured on the flex pipe and its connecting pipe.*

Table 2.4: Mounted sensors at the flex pipe and the connecting pipe.

Measuring location	Number in Figure 2.8
Material temperature of surface	(1)
Material temperature of surface	(1)
Material temperature of surface	(2)
Exhaust gas temperature	(2)
Material temperature of surface	(3)
Material temperature of surface	(4)
Exhaust gas temperature	(4)

2.2 Conducted Measurements

This section describes how the measurements are performed.

2.2.1 Climatic Wind Tunnel Tests

Measurements are performed in a climatic wind tunnel to resemble realistic driving scenarios in various temperatures. In the climatic wind tunnel, mostly stationary points are measured. Tests are performed with three different ambient temperatures, which are -10, 20 and $40°C$.

At the temperature -10 and $40°C$ almost the same type of tests are measured in order to get information of how the surrounding temperature influences the exhaust system. At these temperatures four different engine speeds at 1500, 2500, 3500 and 4500 rpm are tested, at three different engine loads of 50, 100 and 200 Nm. Combining these engine speeds and loads a total of 12 stationary points are obtained. These 12 different stationary points are also measured at three different vehicle velocities which are tried to be kept as close to 50, 100 and 150 km/h as possible. Due to the mechanical connections vehicle speed and engine speed are linked, therefore the gear is selected so that with fixed engine speed the vehicle speed is so close as possible to the targeted.

Another factor that influences the temperature in the exhaust system is the amount of injected fuel into the cylinders. More injected fuel when $\lambda < 1$ will lead to colder exhaust gases since the unburned fuel will have a cooling effect. If $\lambda > 1$ then it will have the opposite effect and the exhaust gas temperature will increase. Tests are therefore performed at predefined stationary points where the value of lambda is changed stepwise from 0.8 until 1.2 with different step lengths.

Scavenging is the process when the burned gases are exchanged by new air/fuel mixture. This happens when both inlet and outlet valves are open simultaneously. This process can improve the engine performance at the same time as it influences the exhaust system temperatures. Tests are therefore made with valve overlap and are changed stepwise as in the fuel/air ratio experiments. Firstly a small valve overlap is present and stepwise this is changed to a bigger overlap until it gets limited by the control system's safety functions.

In order to more easily be able to estimate heat transfer coefficients it can be beneficial to perform cool down experiments. This is done by turning of the engine and cooling it down with a constant wind flow. This was done in the climatic wind tunnel with wind velocities of 160, 120, 80, 40 and 0 km/h. These cool down experiments are done with a surrounding temperature of $-10°C$.

One of the main purposes of the models is to use them to predict temperatures, to enable protection of components like the turbocharger, lambda sensor and catalyst from high temperatures. It is therefore of importance to measure stationary points at maximum brake torque, when the highest temperatures can be reached. This is done with a surrounding temperature of $20°C$. All measurements are saved, including the transient steps in between the stationary points.

2.2.2 Test Track Driving with Brake Trailer

Measurements are also done with the vehicle driving in a real environment, in a test track with a brake trailer. The brake trailer is a device which is attached to the trailer hitch and allows to adjust a desired load. Through this set-up it is possible to simulate slopes and caravan loads. This makes it possible to measure the same stationary points as in the wind tunnel to investigate if the same temperatures are obtained outdoors. Other dynamic tests that are performed in the test track are top speed measurements, aggressive driving, start and stop, running on high engine speeds and cool down experiments. Both shorter and longer pauses are made to simulate for example shopping or dropping the kids at school.

2.3 Challenges with the Measurement

This section describes some challenges that may arise while performing measurements.

2.3.1 Measurement Errors from Radiation and Conduction

Measuring the correct temperature of the exhaust gas can be extremely hard. The thermocouple itself measures its own temperature which is an average temperature of the exhaust gas. Radiation from the inner walls also affects the measurement. When going from higher to lower loads it is possible to obtain incorrect thermocouple readings. The reason for this is that the wall may in some regions be warmer than the exhaust gas, then the thermocouple can give a higher temperature reading due to radiation from the walls and conduction along the probe to the tip of the sensor. In Figure 2.9 the problem with radiation and conduction errors is shown.

Another challenge with temperature measurement is to place the sensor correctly inside the pipe. In order to get faster readings it is beneficial to have the tip of the thermocouple in the middle of the pipe. The aim is to get as much convective heat transfer from the gas as possible.

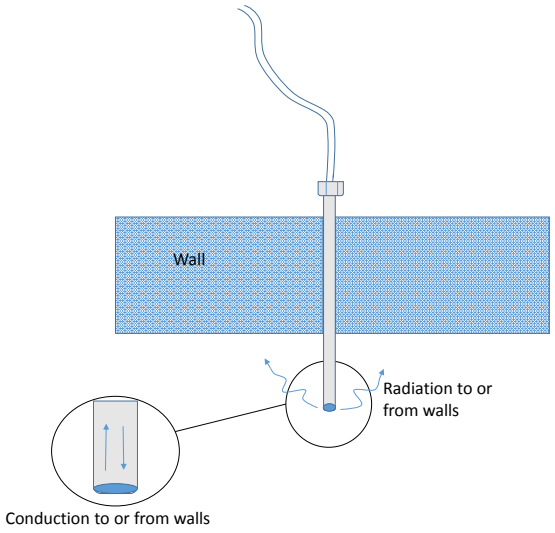

Figure 2.9: *Diagram about possible error that can occur during temperature measurement.*

2.3.2 Challenges with Pulsations

When measuring the exhaust manifold several sensors are placed in different locations. Two sensors are placed in the beginning of the exhaust manifold to measure the outgoing exhaust gas temperature from the cylinders which is shown in Figure 2.4 and Table 2.1. This temperature is used as input signal to the exhaust manifold model and the model itself is validated against the temperature reading before the turbo. However, when measuring in this manner, one does not account for the temperature before the turbo is exposed to more pulsations than the thermocouple in the beginning of the exhaust manifold. The sensor in the end of the manifold gets the contribution from all four cylinders which gives a higher temperature. This assumption is based on simulation made in the exhaust port which is explained in Section 3.3. Since the dynamics of the sensors are not that fast it cannot capture the pulsations in the temperature. It is only possible to measure the average temperature in the beginning of the exhaust manifold and before the turbocharger. In Figure 2.10 this is described with an image.

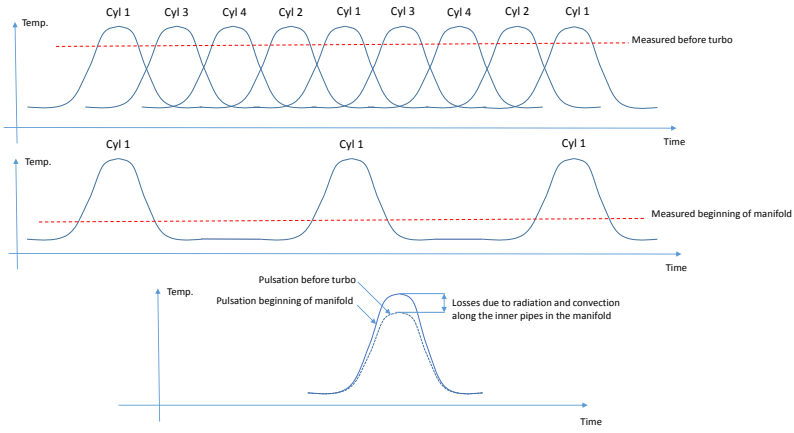

Figure 2.10: *Illustration about how the heat pulsations is present before the turbo and in the beginning of the exhaust manifold.*

In Figure 2.10 it is possible to see that the measured signals are just averaged temperatures since the thermocouple are not fast enough. This makes it harder to model the temperature drop over the manifold, since the pulsations have to be included in order to obtain the correct temperature.

3
Models

This chapter contains the information about the suggested models and information about how the are parameterized.

3.1 Model Parameterization

Volvo cars has developed a program for parameterization in Python. This program automatically imports and joins together all measurement files from a specific folder. The models are implemented in the program in form of discretized equations. Further, the program allows the user to specify which parameters that are constant and which are tunable in the equations. It also allows one to specify boundaries for each tunable parameter to force it to stay in between these specific bounds. The cost function that is used is defined, e.g. $C = (model - measured)^2$. When the parameterization is started the program tries to minimize this cost function by tuning the tunable parameters with different modified optimizations algorithms such as Karush–Kuhn–Tucker conditions and the Levenberg–Marquardt algorithm.

3.2 Cylinder-Out Temperature

The temperature pulsations out from the cylinders are important to study since this temperature is used as input to the exhaust manifold temperature model. The cylinder-out temperature model is only developed theoretically, implementation and validation is left for future work. The modeling of the cylinder-out temperature is divided in to five different stages which are, intake, compression, combustion, expansion and the exhaust stroke. These are shown in Figure 3.1.

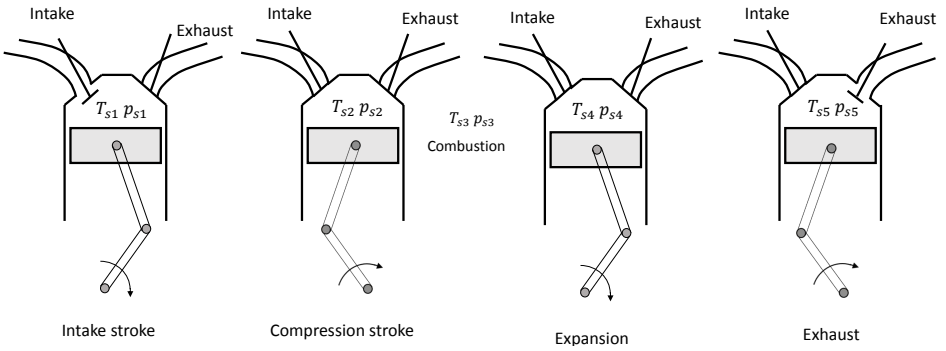

Figure 3.1: *Drawing representing the different stages in the Otto cycle.*

The temperature and pressures are indexed with numbers from one to five in order to facilitate the understanding. These variables are represented in Table 3.1.

Table 3.1: *Indexing of temperatures and pressures inside the cylinder for different parts of the Otto cycle.*

Stage in cycle	Temperature	Pressure
Intake stroke	T_{s1}	p_{s1}
Compression stroke	T_{s2}	p_{s2}
Combustion	T_{s3}	p_{s3}
Expansion stroke	T_{s4}	p_{s4}
Exhaust stroke	T_{s5}	p_{s5}

Intake Stroke

The first stage in the modeling is the intake stroke. In this part the goal is to estimate the temperature in the cylinder when the intake of new air is finished. When trying to evaluate the intake temperature there are some effects that can influence the temperature. Primarily it is needed to account for the remaining residual gases that are left in the cylinder. The remaining residual gases will contribute to a higher temperature and an expression for the amount of residual gases needs to be stated. This is generally known as the residual gas fraction [14], x_r which is calculated by

$$x_{rg} = \frac{m_r}{m_{air} + m_r + m_f} \tag{3.1}$$

where x_{rg} is the residual gas fraction, m_r is the mass of the residual gasses, m_{air} is the mass of the new fresh air entering the cylinder and m_f the mass of injected fuel. The intake stroke temperature T_{s1} [14] is given by the following equation

$$T_{s1} = T_{im}(1 - x_{rg}) + T_r x_{rg} \tag{3.2}$$

where T_r is the residual gas temperature. A first try can be made having m_r and T_r as calibration parameters. In [15] the authors made calculations on x_{rg} for a 2.3 liter four-cylinder SI engine with four valves per cylinder and a variable inlet valve timing. According to their calculations, x_{rg} lies in region between 3.3 % and 33.5 % which can be used as tuning bounds when tuning x_{rg} in (3.2).

If this model does not give as accurate results as desired one can make a more extensive model for the residual gas fraction. In [15] a model for the residual gas fraction x_{rg} is stated. To get an expression of the residual gas fraction it is possible to start with an energy balance at the inlet valve closing

$$m_{cyl1} c_{v,cyl} T_{ivc} = m_{air} c_{v,air} T_{im} + m_r c_{v,r} T_r \tag{3.3}$$

It is further assumed that the mass of fuel is a part of the mass of the residuals.

$$x_{rg} = \frac{m_r}{m_{air} + m_r + m_f} \approx \frac{m_r}{m_{air} + m_r} = \frac{m_r}{m_{cyl1}} \Leftrightarrow x_{rg} m_{cyl1} = m_r \tag{3.4}$$

The specific heat for the content in the cylinder can be expressed as follows

$$c_{v,cyl} = (1 - x_{rg}) c_{v,air} + x_{rg} c_{v,r} \tag{3.5}$$

It is now possible to simplify the residual gas fraction with the help of (3.3) - (3.5), which results in

$$x_{rg} = \frac{c_{v,air}(T_{ivc} - T_{im})}{c_{v,air}(T_{ivc} - T_{im}) + c_{v,r}(T_r - T_{ivc})} \tag{3.6}$$

The residual gas temperature depends on the wall temperatures, the combustion, the engine speed and the mass flow. The authors in [15] discovered that engine speed and the total mass in the cylinder are the two most important variables. They developed the following model for the residual gas temperature

$$T_r = -(c_{r1}(m_{cyl1} N))^{c_{r2}} + c_{r3} \tag{3.7}$$

where c_{r1}, c_{r2} and c_{r3} are tuning parameters. These tuning parameters can be found in the same way as in [26]. Furthermore the values of $c_{v,air}$ and $c_{v,r}$ can be found in thermodynamic tables. The temperature at IVC T_{ivc} can be computed through the ideal gas law

$$T_{ivc} = \frac{p_{s1} V_{ivc}}{R_{ivc} m_{cyl1}} \tag{3.8}$$

A simplification is made so that the mass of the air inside the cylinder can be computed through the density, volume at IVC and the residual gas fraction. The equation for the simplified mass calculation is given by

$$m_{cyl1} = \frac{m_{air}}{1 - x_{rg}} = \frac{\rho_{air} V_{ivc}}{1 - x_{rg}} \tag{3.9}$$

If this simplification results in m_{cyl1} not being accurate enough a more thorough method is presented in [15]. Further the gas constant at IVC can be computed as

$$R_{ivc} = R_r x_{rg} + R_{air}(1 - x_{rg}) \tag{3.10}$$

where the values for R_r and R_{air} can be found in tables. Furthermore, by combining (3.8)-(3.10) the temperature at IVC can be described by

$$T_{ivc} = \frac{p_{s1} V_{ivc}}{\left(R_r x_{rg} + R_{air}(1 - x_{rg})\right) \frac{\rho_{air} V_{ivc}}{1 - x_{rg}}} \tag{3.11}$$

The residual gas fraction can now be estimated by making an initial guess of x_{rg} thereafter m_{cyl1} and T_{ivc} can be calculated. The temperature T_{ivc} should then be used in (3.6) to compute a new value of x_{rg}. If this new value does not correspond to the initial guess, x_{rg} obtains a new value. This procedure continues until the x_{rg} value converges. An overview of this process is presented in Figure 3.2.

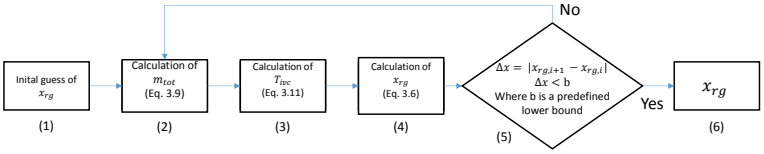

Figure 3.2: *Iteration steps for residual gas fraction estimation.*

The amount of residual gases that are left in the cylinder are also influenced by the inlet and outlet valves. An early closing of the exhaust valve results in a higher amount of residual gases and increases the in-cylinder temperature. In the same manner the temperature decreases when internal scavenging occurs. During internal scavenging there is valve overlap present which allows fresh air to flow through the cylinders and into the exhaust manifold if the pressure in the intake manifold is greater than the exhaust manifold pressure. Back flow also exist, which occurs when the pressure in the exhaust manifold is higher. Exhaust gases are at that point pushed into the cylinder and a higher in-cylinder temperature is obtained due to increased amount of residual gases. These effects are not considered in the proposed model but if an extensive model is developed this may be valuable to include.

Another issue is that the pressure in the cylinder is required to compute the compression pressure p_{s2}. There are different alternatives to model the pressure at

IVC. Here are three different models suggested in [10]. The pressure at IVC can be set equal to intake manifold pressure at valve closing

$$p_{ivc} \approx p_{im}(\theta_{ivc}) \approx p_{s1} \tag{3.12}$$

Another way is to model the pressure as a factor of the intake manifold pressure

$$p_{ivc} = p_{im}(\theta_{ivc})c_1 = p_{s1} \tag{3.13}$$

A third model is suggested with two parameters

$$p_{ivc} = p_{im}(\theta_{ivc}) + c_1 + c_2 N = p_{s1} \tag{3.14}$$

According to [10] the model with one parameter, (3.13), gives sufficient accuracy. The model with two parameters, (3.14), gives higher accuracy but makes the model more complex.

All parameters used in (3.1)-(3.14) are described in Table 3.2.

Finally the collected equations for modeling the intake stroke look as follows

$$T_{s1} = T_{im}(1 - x_{rg}) + T_r(x_{rg})$$

x_{rg} and T_r can either be left as tuning parameters or modeled with

$$x_{rg} = \frac{c_{v,air}(T_{s1} - T_{im})}{c_{v,air}(T_{s1} - T_{im}) + c_{v,r}(T_r - T_{s1})}$$

$$T_r = -(c_{r1}(m_{cyl1}N))^{c_{r2}} + c_{r3}$$

$$T_{s1} = \frac{p_{s1}V_{ivc}}{\left(R_r x_{rg} + R_{air}(1 - x_{rg})\right)\frac{\rho_{air}V_{ivc}}{1-x_{rg}}}$$

Compression

The compression that takes place after the intake stroke can be seen as an isentropic process. The change in pressure can be computed with the help of change in volume. The temperature in the compression stroke can be found in [14] and is given by

$$T_{s2}(\theta) = T_{s1}(\theta_{ivc})\left(\frac{V(\theta_{ivc})}{V(\theta)}\right)^{\gamma-1} \tag{3.15}$$

and the corresponding pressure is described by

$$p_{s2}(\theta) = p_{s1}(\theta_{ivc})\left(\frac{V(\theta_{ivc})}{V(\theta)}\right)^{\gamma} \tag{3.16}$$

where γ is the polytropic exponent.

Combustion

In order to compute the temperature during the combustion phase it is possible to use the ideal gas law. By differentiation of the ideal gas law it is possible to

obtain an expression for the temperature change in the cylinder

$$m_{cyl1} R T_{s3} = p_{s3} V \Leftrightarrow dT_{s3} = \frac{dp_{s3} V}{m_{cyl1} R} + \frac{p_{s3} dV}{m_{cyl1} R} \tag{3.17}$$

The gas constant and the specific heat, are known parameters

$$R = c_p - c_v \tag{3.18}$$

$$c_v = \frac{\gamma - 1}{\gamma} \tag{3.19}$$

The volume change as a function of the crank angle is derived in [14] and is described by

$$V(\theta) = V_d \left[\frac{1}{r_c - 1} + \frac{1}{2} \left(\frac{l}{a_{rad}} + 1 - \cos(\theta) - \sqrt{\left(\frac{l}{a_{rad}} \right)^2 - \sin^2(\theta)} \right) \right] \tag{3.20}$$

Where l is the connecting rod length, a_{rad} is the crank radius, V_d is the displacement and r_c is the compression ratio. Furthermore, the derivative with respect to the crank angle for the volume is given by

$$\frac{dV(\theta)}{d\theta} = \frac{1}{2} V_d \sin\theta \left(1 + \frac{\cos\theta}{\sqrt{\left(\frac{l}{a}\right)^2 - \sin^2\theta}} \right) \tag{3.21}$$

Further, the pressure change in the cylinder needs to be calculated. This is done by studying the internal energy. The change in internal energy can be described using the first law of thermodynamics as the change in heat and the work performed on the closed system

$$dU = dQ_{heat} - dW \tag{3.22}$$

The change of heat in the closed system is divided into the heat release from the fuel and the heat that disappears through the cylinder walls

$$dU = \underbrace{dQ_{hr} - dQ_{ht}}_{dQ_{heat}} - dW \tag{3.23}$$

where Q_{hr} is the heat release from the fuel and Q_{ht} is the heat transfer through the walls. The change in internal energy can be described with the specific internal energy and the mass of the content inside the cylinder

$$U = mu \tag{3.24}$$

From this equation it is possible to derive an expression for the temperature change in the cylinder which is found in [14]

$$dT = -\frac{(\gamma - 1) RT}{V} dV + \frac{1}{m c_v} (dQ_{hr} - dQ_{ht}) \tag{3.25}$$

By combining (3.17)-(3.19) it is possible to rewrite (3.25) and get an expression of the pressure change in the cylinder as follows

$$dp = -\frac{\gamma p}{V} dV + \frac{\gamma - 1}{V} (\underbrace{dQ_{hr} - dQ_{ht}}_{\text{Need to be estimated}}) \tag{3.26}$$

In order to compute the pressure change in the cylinder expressions for the change in heat release dQ_{hr} and the heat transfer to cylinder walls dQ_{ht} are required. The heat release is usually described with a normalized function called mass fraction burned. This function describes the combustion with the help of parameters such as ignition timing and flame development angle which is defined as the period from start of combustion until when 10 % of the mass has burnt. Another parameter that is included in this function is the rapid burning angle which is the interval of crank angles from when 10 % until 90 % of the mass has burnt. This is called the Vibe function x_b and is found in [14]

$$x_b(\theta) = 1 - e^{-a\left(\frac{\theta - \theta_{ign}}{\Delta\theta}\right)^{m+1}} \tag{3.27}$$

Where θ is the crank angle, θ_{ign} is the angle for which the combustion starts. The parameter m influence the shape of the burning profile. A higher value on m gives an earlier combustion. The parameters a and $\Delta\theta$ are connected to the combustion duration, where a that also is found in [14] is described by

$$a = -\ln(1 - 0.1)\left(\frac{\Delta\theta}{\Delta\theta_d}\right)^{m+1} \tag{3.28}$$

and $\Delta\theta_d$ is the flame development angle. The angle $\Delta\theta_d$ describes when $0 - 10\%$ mass fraction is burnt and $\Delta\theta_b$ describes when $10 - 85\%$ mass fraction is burnt. If $\Delta\theta_d$ and $\Delta\theta_b$ are known it is possible to write the parameter m as in [14]

$$m = \frac{\ln\left(\frac{\ln(1-0.1)}{\ln(1-0.9)}\right)}{(\ln(\Delta\theta_d) - \ln(\Delta\theta_d + \Delta\theta_b))} - 1 \tag{3.29}$$

Due to overestimation it is according to [14] necessary to specify either a or $\Delta\theta$ for an unique solution. Furthermore $\Delta\theta$ can be approximated by

$$\Delta\theta \approx 2 \cdot \Delta\theta_d + \Delta\theta_b \tag{3.30}$$

Now it is possible to make an expression for the heat release

$$\frac{dQ_{hr}(\theta)}{d\theta} = \underbrace{m_f \cdot q_{LHV}}_{\text{Energy content in fuel}} \cdot \underbrace{\eta_c}_{\text{Combustion efficiency}} \cdot \underbrace{\frac{dx_b(\theta)}{d\theta}}_{\text{Combustion process}} \tag{3.31}$$

The chemical energy in the cylinder can be described with the mass of the fuel m_f and the lower heating value q_{LHV}. In some operating conditions when the fuel-air mixture becomes rich it is not possible to extract all chemical energy from the fuel and therefore an efficiency term is added to include the energy that is not

converted

$$\eta_c(\lambda) = \min(1, \lambda) \tag{3.32}$$

The pressure in the cylinder in (3.26) is influenced by the specific heat ratio for the gas and fuel mixture. It decreases when the temperature rises. The specific heat ratio can be modeled in many ways, here it is described by a model suggested in [11] given by

$$\gamma(T) = \gamma_{300} - b(T - 300) \tag{3.33}$$

Where γ_{300} is the specific heat for 300 K which lies around 1.35. The parameter b decides the linear slope which is left as a tuning parameter. Since the cylinder is a closed system during the combustion the mass can be computed through (3.9) or with

$$m_{cyl2} = \frac{p_{ivc} V_{ivc}}{R T_{ivc}} \tag{3.34}$$

Finally the collected equations for the modeling of the combustion is given by

$$T(\theta) = \frac{p_{s3}(\theta)V(\theta)}{m_{cyl2}R} \tag{3.35}$$

$$\frac{dp_{s3}(\theta)}{d\theta} = -\frac{\gamma(T)\cdot p_{s3}(\theta)}{V(\theta)}\frac{dV}{d\theta} + \frac{\gamma(T)-1}{V(\theta)}\left(\frac{dQ_{hr}}{d\theta} - \frac{dQ_{ht}}{d\theta}\right) \tag{3.36}$$

The pressure p_{s3} can be integrated from the expression above. A initial pressure can be obtained from (3.16)

$$\gamma(T) = \gamma_{300} - b(T-300) \tag{3.37}$$

$$V(\theta) = V_d\left[\frac{1}{r_c-1} + \frac{1}{2}\left(\frac{l}{a_{rad}} + 1 - \cos(\theta) - \sqrt{\left(\frac{l}{a_{rad}}\right)^2 - \sin^2(\theta)}\right)\right] \tag{3.38}$$

$$\frac{dV(\theta)}{d\theta} = \frac{1}{2}V_d\sin\theta\left(1 + \frac{\cos\theta}{\sqrt{\left(\frac{l}{a}\right)^2 - \sin^2\theta}}\right) \tag{3.39}$$

$$\frac{dQ_{hr}(\theta)}{d\theta} = m_f q_{LHV}\eta_c\frac{dx_b}{d\theta}(\theta) \tag{3.40}$$

$$\eta_c = \min(\lambda, 1) \tag{3.41}$$

$$x_b(\theta) = 1 - e^{-a\left(\frac{\theta-\theta_{ign}}{\Delta\theta}\right)^{m+1}} \tag{3.42}$$

$$\Delta\theta \approx 2\cdot\Delta\theta_d + \Delta\theta_b \tag{3.43}$$

$$m = \frac{\ln\left(\frac{\ln(1-0.1)}{\ln(1-0.9)}\right)}{(\ln(\Delta\theta_d) - \ln(\Delta\theta_d + \Delta\theta_b))} - 1 \tag{3.44}$$

$$a = -\ln(1-0.1)\left(\frac{\Delta\theta}{\Delta\theta_d}\right)^{m+1} \tag{3.45}$$

The term $\frac{dQ_{ht}}{d\theta}$ can be left as a tuning parameter or a state of the wall can be made so that the losses through the walls can be computed.

Expansion

The expansion can be seen as an isentropic process similar to the compression which can be found in [14]. Where the temperature is given by

$$T_{s4} = T_{s3}\left(\frac{V_{c3}}{V(\theta)}\right)^{1-\frac{1}{\gamma}} \tag{3.46}$$

and the pressure by

$$p_{s4} = p_{s3}\left(\frac{V_{c3}}{V(\theta)}\right)^{\gamma} \tag{3.47}$$

Blowdown

The blowdown takes place when the exhaust valve opens and the content in the cylinder is pushed out into the manifold. The pressure in the cylinder drops to exhaust manifold pressure and the temperature in the cylinder becomes equal to the temperature in the exhaust manifold. Some heat is transferred to the exhaust valves due to the high temperatures and velocities which can be modeled but is not done here. The temperature during the blowdown is found in [14]

$$T_{s5} = T_{s4}\left(\frac{p_{em}}{p_{s4}}\right)^{1-\frac{1}{\gamma}} \tag{3.48}$$

All parameters in this section are described further in Table 3.2.

Table 3.2: *Nomenclature for the cylinder-out model.*

Notation	Description	Unit
a, m	Tuning parameters for the vibe function	$[-]$
a_{rad}	Crank radius	$[m]$
b	Tuning parameter for specific heat model	$[-]$
c_1, c_2	Tuning parameters for intake manifold pressure model	$[-]$
c_{r1}, c_{r2}, c_{r3}	Tuning parameters for residual gas temperature model	$[-]$
c_p	Specific heat	$[\frac{J}{KgK}]$
c_v	Specific heat for a constant volume	$[\frac{J}{KgK}]$
$c_{v,air}$	Specific heat of air inside the cylinder	$[\frac{J}{KgK}]$
$c_{v,r}$	Specific heat of residual gases inside the cylinder	$[\frac{J}{KgK}]$
$c_{v,cyl}$	Specific heat of mixture inside the cylinder	$[\frac{J}{KgK}]$
$\Delta\theta$	Burning duration	$[^\circ]$
η_c	Combustion efficiency	$[-]$
γ	Polytropic exponent	$[-]$
γ_{300}	Specific heat for air at 300 K	$[\frac{J}{Kg}]$
l	Length of connecting rod	$[m]$
λ	Air/fuel ratio	$[-]$
m_{cyl1}	Model 1 for total mass in cylinder	$[Kg]$
m_{cyl2}	Model 2 for total mass in cylinder	$[Kg]$
m_f	Mass of injected fuel	$[Kg]$
m_r	Mass residual gas in cylinder	$[Kg]$
N	Engine speed	$[rps]$

p_{im}	Pressure intake manifold	$[Pa]$
p_m	Motorized pressure	$[Pa]$
p_{s1}	Pressure during intake stroke	$[Pa]$
p_{s2}	Pressure during compression stroke	$[Pa]$
p_{s3}	Pressure during the combustion	$[Pa]$
p_{s4}	Pressure during the expansion stroke	$[Pa]$
p_{s5}	Pressure during the exhaust stroke	$[Pa]$
q_{LHV}	Lower heating value	$[\frac{J}{Kg}]$
$\dot{Q}_{c,air}$	Convective heat transfer from/to cylinder walls	$[W]$
Q_{heat}	Change in heat inside cylinder during combustion	$[J]$
Q_{hr}	Heat release from combustion	$[J]$
Q_{ht}	Heat transfer to cylinder walls	$[J]$
r_c	Compression ratio	$[-]$
R	Gas constant	$[\frac{J}{KgK}]$
R_{air}	Gas constant of air inside the cylinder	$[\frac{J}{KgK}]$
R_{ivc}	Gas constant at inlet valve closing	$[\frac{J}{KgK}]$
R_r	Gas constant of residual gases inside the cylinder	$[\frac{J}{KgK}]$
ρ_{air}	Density of air inside the cylinder	$[\frac{Kg}{m^3}]$
T_{im}	Intake manifold temperature	$[K]$
T_{ivc}	Temperature at inlet valve closing	$[K]$
T_r	Residual gas temperature	$[K]$
T_{s1}	Temperature during intake stroke	$[K]$
T_{s2}	Temperature during compression stroke	$[K]$
T_{s3}	Temperature during combustion	$[K]$
T_{s4}	Temperature during the expansion stroke	$[K]$
T_{s5}	Temperature during the exhaust stroke	$[K]$
θ	Crank angle	$[°]$
θ_b	Fast burn angle	$[°]$
θ_d	Flame development angle	$[°]$
θ_{ivc}	Crank angle at inlet valve closing	$[°]$
u	Specific internal energy	$[\frac{J}{Kg}]$
U	Internal energy	$[J]$
V	Volume inside cylinder	$[m^3]$
V_{c3}	Cylinder volume during combustion	$[m^3]$
V_d	Cylinder displacement	$[\frac{m^3}{rev}]$
V_{ivc}	Volume at inlet valve closing	$[m^3]$
W	Work performed from expansion	$[J]$
x_b	Mass burned fraction	$[-]$
x_{rg}	Residual gas fraction	$[-]$

3.3 Exhaust Manifold

The exhaust manifold modeled in this project is a dual wall manifold, a diagram is shown in Figure 2.1. This means that it is constructed of two different layers. The first layer consists of four inner pipes and the second layer consists of one covering surface around all four pipes.

The energy balance for a control volume of the exhaust manifold is shown in Figure 3.3 where the square shows the energy transfers from one segment and the energies in the circle shape describes the energy transfers from the inner wall out to the ambient.

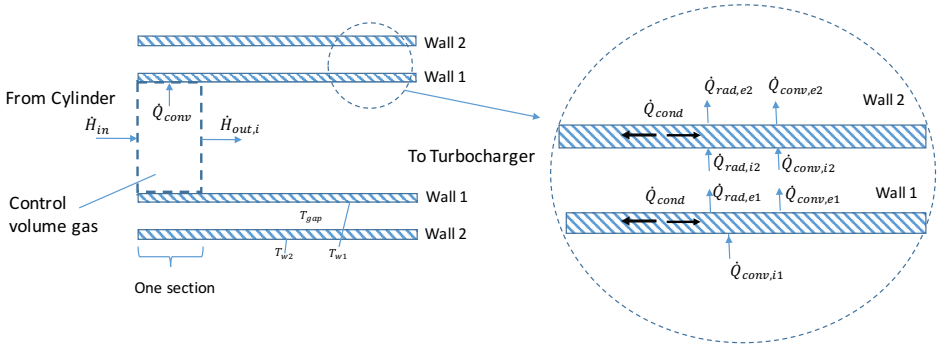

Figure 3.3: *Diagram about the different layers in the exhaust manifold. It illustrates a pipe with dual walls and how the energy is transferred between the layers.*

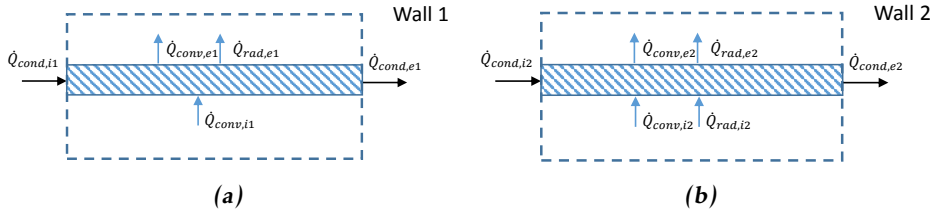

Figure 3.4: *Shows the energy balance for the first and second wall. Where* ***(a)*** *shows the first wall and* ***(b)*** *shows the second wall.*

Figure 3.4a shows the energy balance for the first wall where inflow of energy to the wall is obtained by convection from the hot exhaust gas and conduction along the pipe. The figure also shows the outflow of energy from the wall which can be written in terms of radiation, convection and conduction. Inspiration was gathered from [22, 9] in order to form an energy balance between the exhaust gas

and the first wall, T_{w1} is described by

$$m_g c_{p,g} \frac{dT_{gas}}{dt} = \dot{m}_g c_{p,g} b \frac{\partial T_{gas}}{\partial z} - h_{gi} A_{ir} (T_{gas} - T_{w1}) \tag{3.49}$$

where z is the axial position. Further, the first term on the right hand side accounts for the convective heat transfer and the second term for the heat exchange between the exhaust gas and the first wall. The wall temperature is described by the following PDE

$$\begin{aligned} m_{w1} c_{p,w1} \frac{dT_{w1}}{dt} = A_{ir} h_{gi} \left(T_{gas} - T_{w1} \right) + k_{cde} A_{cde1} \frac{\partial^2 T_{w1}}{\partial z^2} - \\ A_{or} h_{cve} \left(T_{w1} - T_{gap} \right) - A_{or} F_v \epsilon \sigma \left(T_{w1}^4 - T_{w2}^4 \right) \end{aligned} \tag{3.50}$$

where the first term on the right hand side accounts for the convective heat transfer between the gas and the inner wall. The second term describes the thermal conduction which occurs along the wall material. Furthermore, the third term describes the convective heat transfer between the wall and the gap. In addition to that the temperature of the outside of the wall is assumed to be equal to the temperature of the inside due to the high conductivity of metal. Finally the last term accounts for the radiation between the first and the second layer. The temperature in the gap, T_{gap} is described by

$$m_{gap} c_{p,g} \frac{dT_{gap}}{dt} = h_{w2g} A_{ir} (T_{w1} - T_{gap}) - h_{g2w} A_{or} (T_{gap} - T_{w2}) \tag{3.51}$$

where the first term on the right hand side accounts for the heat obtained from the first wall and the second term for the heat lost to the second wall. The corresponding energy balance for the second wall is shown in Figure 3.4b. The wall temperature for the second wall, T_{w2} in (3.50) is described by the following PDE

$$\begin{aligned} m_{w2} c_{p,w2} \frac{dT_{w2}}{dt} = A_{iw2} h_{g2w2} \left(T_{gap} - T_{w2} \right) + k_{cde2} A_{cde2} \frac{\partial^2 T_{w1}}{\partial z^2} + \\ A_{or} F_v \epsilon \sigma \left(T_{w1}^4 - T_{w2}^4 \right) - A_{ow2} h_{cve2} \left(T_{w2} - T_{amb} \right) - A_{ow2} F_v \epsilon \sigma \left(T_{w2}^4 - T_{amb}^4 \right) \end{aligned} \tag{3.52}$$

where the description of the terms are similar to the one for (3.50). The derivation of (3.49)-(3.52) is inspired by the approaches in [22, 9]. Since these equations consists of PDEs the equations are discretized to be applicable in the ECM. However since the dynamics of gas temperature are much faster than the dynamics of the wall temperatures, T_{gas} can be approximated to be in steady state, which results in the left hand side in (3.49) being set to zero. Further the first term on the right hand side in that equation is discretized in the axial direction by using forward difference. Which results in the gas temperature being described by

$$T_{gas}^{(k)} = \frac{\dot{m}_g c_{p,g} T_{gas}^{(k-1)} - \frac{A_{ir}}{N} h_{gi} T_{w1}}{\dot{m}_g c_{p,g} - h_{gi} \frac{A_{ir}}{N}} \tag{3.53}$$

where k is the current control volume and N the total amount of control volumes.

The gap temperature is calculated in the same way and is given by

$$T_{gap} = \frac{h_{w2g}A_{ir}T_{w1} + h_{g2w}A_{or}T_{w2}}{h_{g2w}A_{or} + h_{w2g}A_{ir}} \tag{3.54}$$

The time derivative in (3.50) is discretized by using Euler forward since it is the most simple solution. The equation also consists of a second order PDE, which is solved by using the finite central method. This results in T_{w1} being described by

$$T_{w1}^{(k)}(i) = T_{w1}^{(k)}(i-1) + T_s\frac{dT_{w1}^{(k)}(i-1)}{dt} \tag{3.55}$$

where i is the current sample. The derivative for the wall temperature is given by

$$\frac{dT_{w1}^{k}(i)}{dt} = \frac{1}{\frac{m_{w1}}{N}c_{p,w1}}\left[\frac{A_{ir}}{N}h_{gi}\left(T_{gas}^{k} - T_{w1}^{k}\right) + k_{cde}A_{cde1}\frac{T_{w1}^{k-1}(i) - 2T_{w1}^{k}(i) + T_{w1}^{k+1}(i)}{\frac{L}{N}} - \right.$$
$$\left. \frac{A_{or}}{N}h_{cve}\left(T_{w1}^{k} - T_{gap}^{k}\right) - F_v\epsilon\sigma\frac{A_{or}}{N}\left(T_{w1}^{4^k}(i) - T_{w2}^{4^k}(i)\right)\right] \tag{3.56}$$

where k is the current segment and N is the total amount of segments. According to [9] the engine block acts as a heat sink. Heat is transferred along the exhaust manifold into the engine block. This was also confirmed by the measurements. This means that the conduction term for $k = 0$ should be set to the engine block temperature. Furthermore, the temperature for the second wall is given by

$$T_{w2}^{(k)}(i) = T_{w2}^{(k)}(i-1) + T_s\frac{dT_{w2}^{(k)}(i-1)}{dt} \tag{3.57}$$

where the derivative is given by

$$\frac{dT_{w2}^{k}(i)}{dt} = \frac{1}{\frac{m_{w2}}{N}c_{p,w2}}\left[\frac{A_{iw2}}{N}h_{g2w2}\left(T_{gap}^{k} - T_{w2}^{k}\right) + \right.$$
$$k_{cde2}A_{cde2}\frac{T_{w2}^{k-1}(i) - 2T_{w2}^{k}(i) + T_{w2}^{k+1}(i)}{\frac{L}{N}} + \frac{A_{or}}{N}F_v\epsilon\sigma\left(T_{w1}^{4^k} - T_{w2}^{4^k}\right) - \tag{3.58}$$
$$\left.\frac{A_{ow2}}{N}h_{cve2}\left(T_{w2}^{k} - T_{amb}^{k}\right) - \frac{A_{ow2}}{N}F_v\epsilon\sigma\left(T_{w2}^{4^k} - T_{amb}^{4}\right)\right]$$

All parameters from the equations in this section are described in Table 3.3. In addition to that the exhaust manifold consists of four different pipes, which makes it necessary to model each pipe separately and then join them together before the turbocharger. This is necessary to do since pulsations occur in the pipes. These pulsations make the temperature higher before the turbocharger as described in Section 2.3.2. In order to capture this behavior it would be required to have a crank angle based temperature signal as input. Unfortunately, crank based measurements were not possible. Due to that, the proposed model cannot be validated. One suggestion for solving this issue could be to look at data from exhaust

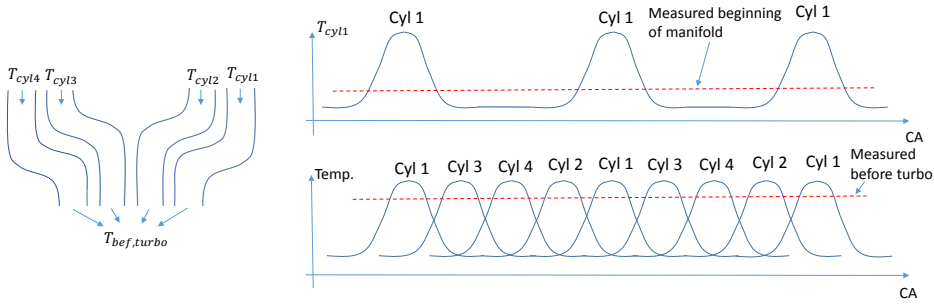

Figure 3.5: *Illustration about how the pulsations from the different pipes conduct in higher temperature before the turbocharger.*

port simulations where one can see how the temperature is changing when the exhaust valve opens and closes. When the exhaust port opens a peak in temperature is obtained and when it is closed the temperature lies around a constant level. Knowing the appearance of the temperature it is possible to use the measured signal in the exhaust port to construct a crank angled based signal. The measured signal is sampled with 10 Hz but can be resampled and reconstructed so that it captures the behavior from the pulsations. From simulations (Figure 3.6) it is possible to get a feeling of the amplitude of the peaks and temperature level when the valve is open and closed.

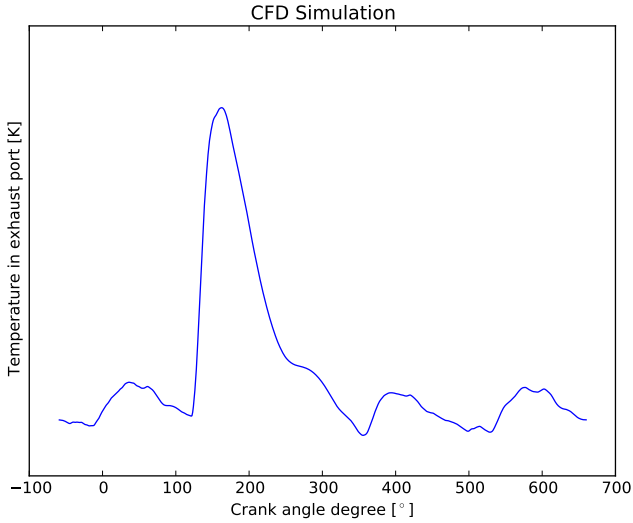

Figure 3.6: *CFD simulation of one combustion cycle in the exhaust port of one cylinder. The scale on the y-axis is here removed due to confidentiality reasons.*

Using the information from Figure 3.6 it is possible to construct an artificial square signal, see Figure 3.7. From 3.6 it is also possible to see that the temperature oscillates from around 350 to 100 crank angle degrees. This is probably due to the fact that the pulsations bounces back and forward in the pipes. When constructing the artificial square wave signal this behavior is ignored and approximated with a constant level.

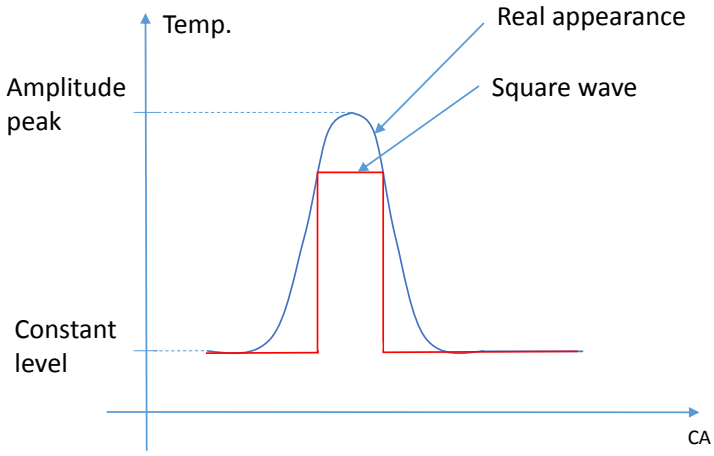

Figure 3.7: *Illustration about how the pulsation can be reconstructed as a square wave.*

This constructed wave signal can then be used as input to the exhaust temperature model. Finally one will end up having four shifted square waves which will be averaged in the same manner as in Figure 3.5. This will hopefully give a more realistic input to the model so that the modeled temperature before the turbo agree better to the measured temperature. Unfortunately this was not tested due to time limitations.

Table 3.3: *Nomenclature for the exhaust manifold model.*

Notation	Description	Unit
A_{cde1}	Cross section area of the material of wall 1	$[m^2]$
A_{cde2}	Cross section area of the material of wall 2	$[m^2]$
A_{ir}	Inner area of wall 1	$[m^2]$
A_{iw2}	Inner area of wall 2	$[m^2]$
A_{or}	Outer area of wall 1	$[m^2]$
A_{ow2}	Outer area of wall 2	$[m^2]$
b	Thickness of a segment	$[m]$
$c_{p,w1}$	Specific heat capacity of wall 1	$[\frac{J}{kgK}]$
$c_{p,w2}$	Specific heat capacity of wall 2	$[\frac{J}{kgK}]$
$c_{p,g}$	Exhaust gas	$[\frac{J}{kgK}]$
ϵ	Emissivity of wall	$[-]$
F_v	View factor	$[-]$
h_{cve1}	Convective heat transfer coefficient from outer area of wall 1 to air in the gap	$[\frac{W}{m^2K}]$
h_{cve2}	Convective heat transfer coefficient from outer area of wall 2 to ambient	$[\frac{W}{m^2K}]$
h_{g2w2}	Convective heat transfer coefficient from air in gap to wall 2	$[\frac{W}{m^2K}]$
h_{w2g}	Convective heat transfer coefficient from gap to wall 2	$[\frac{W}{m^2K}]$
h_{gi}	Convective heat transfer coefficient from exhaust gas to inner walls	$[\frac{W}{m^2K}]$
h_{w2g}	Convective heat transfer coefficient from wall 1 to gap	$[\frac{W}{m^2K}]$
k_{cde1}	Thermal conductivity of wall 1	$[\frac{W}{mK}]$
k_{cde2}	Thermal conductivity of wall 2 $[\frac{W}{mK}]$	
m_g	Mass of exhaust gas	$[kg]$
$\dot{m}_g$	Exhaust gas mass flow	$[kg/s]$
m_{gap}	Mass of gas between the walls	$[kg]$
m_{w1}	Mass of wall 1	$[kg]$
m_{w2}	Mass of wall 2	$[kg]$
N	Number of segments	$[-]$
σ	Stefan-Boltzmann's constant	$[\frac{W}{m^2K^4}]$
T_{amb}	Temperature of ambient air	$[K]$
T_{gap}	Temperature in the gap between the walls	$[K]$
T_{gas}	Temperature of the exhaust gas	$[K]$
T_{w1}	Temperature of the inner wall (Wall 1)	$[K]$
T_{w2}	Temperature of the outer wall (Wall 2)	$[K]$

3.4 Turbocharger

The main purpose of the turbine side of the turbocharger is to extract energy from the exhaust gas with higher pressure and temperature and deliver it as work to the compressor. A full energy balance for the turbine side of the turbocharger is shown in Figure 3.8. The enthalpy entering the system is presented by $\dot{H}_{in}$.

Some heat is transferred by convection to the solid parts of the turbine which is named $\dot{Q}_{conv,solid}$. This heat is further transported to the compressor side through the shaft by conduction which is denoted $\dot{Q}_{cond}$. The extracted work by the turbine is presented by $\dot{W}$. The absorbed energy by the body housing is denoted $\dot{Q}_{conv,BH}$. The energy from the body housing is further transported to the ambient by convection and radiation which are denoted $\dot{Q}_{rad}$ and $\dot{Q}_{conv}$ in Figure 3.8. Furthermore, some energy is also absorbed by the oil and water circulating in the turbocharger, this energy is denoted by $\dot{Q}_{oil+water}$ in the Figure. The enthalpy in the exhaust gas leaving the system is denoted $\dot{H}_{out}$.

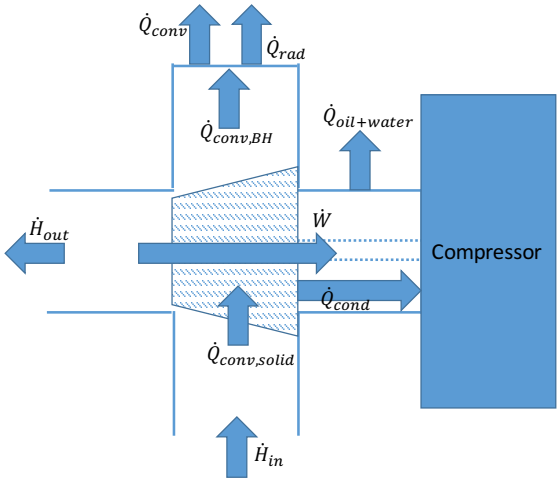

Figure 3.8: *Diagram about the energy balance for the turbine side of the turbocharger.*

However, some simplifications are made from the energy balance in Figure 3.8. Since the wall temperature is not measured, the energy loss by radiation is included in the convection term instead. Since the estimation would not be accurate enough. Furthermore the heat loss to the oil and water is not that big according to [24], therefore the heat loss to the oil and water are simplified from the energy balance. In addition to this it is very hard to estimate the heat loss to the compressor side and thereby this term is not modeled separately, instead it is included in the other energy losses, this for instance can lead to a higher estimation of the turbine efficiency. The simplified energy balance that is used for the modeling is shown in Figure 3.9.

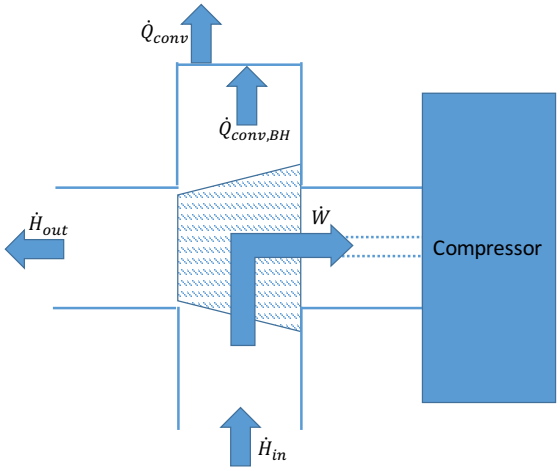

Figure 3.9: *The simplified diagram about the energy balance for the turbine side of the turbocharger.*

To implement the energy balance in Figure 3.9 the balance is divided into a state for the gas phase and a second state for the solid phase. The gas phase for a control volume is described by

$$m_g c_{p,g} \frac{T_g}{dt} = \dot{m}_{exh} c_{p,g} (T_{in} - T_g) + h_{sg} A_{sg} (T_{sol} - T_g) - \dot{W} \tag{3.59}$$

where the first term on the right hand side accounts for the convective heat transfer in the axial direction and the second term for the heat exchange between the gas and the solid. The work extracted by the turbine is denoted $\dot{W}$. However, since the dynamics of the gas phase are much faster than the dynamics of the body housing, the gas phase T_g can be approximated to be in steady state. This means that the left hand side in (3.59) can be set to zero, thereby the equation can be rewritten as

$$T_g = \frac{\dot{m}_{exh} c_{p,g} T_{in} + h_{sg} A_{sg} T_{sol} - \dot{W}}{\dot{m}_{exh} c_{p,g} + h_{sg} A_{sg}} \tag{3.60}$$

The state for the body housing temperature, T_{sol} is described as

$$m_{sol} c_{p,sol} \frac{dT_{sol}}{dt} = h_{sg} A_{sg} \left(T_g - T_{sol} \right) + h_{sa} A_{sa} \left(T_{amb} - T_{sol} \right) \tag{3.61}$$

where the first term on the right hand side describes the heat exchange between the exhaust gas and the solid. The second term on that side accounts for the convective heat exchange between the body housing and the ambient. The equation is further discretized in the time domain by implementing the Euler forward

method. By doing so the temperature of the body housing is given by

$$T_{sol}(i) = T_{sol}(i-1) + T_s \frac{T_{sol}(i-1)}{dt} \tag{3.62}$$

where i is the current sample and T_s the sample time. The energy converted to work by the turbine, $\dot{W}$ in (3.59) according to [14], is described by

$$\dot{W} = \dot{m}_{turb} c_{p,g} T_{in} \eta_t \left(1 - \left(\frac{p_{aft}}{p_{bef}} \right)^{\frac{\gamma-1}{\gamma}} \right) \tag{3.63}$$

The mass flow through the turbine is here denoted $\dot{m}_{turb}$. The work is based on the pressure ratio between the pressures before and after the turbine. Turbine efficiency, η_t, is calculated as

$$\eta_t = k_0 \left(1 - \left(\frac{\text{BSR} - k_1}{k_1} \right)^2 \right) \tag{3.64}$$

where k_0 and k_1 are tuning parameters. The blade speed ratio, BSR which gives information about the ratio between the speed of the exhaust gas in comparison to the speed of the turbine is given by

$$\text{BSR} = \frac{r_t \omega_t}{\sqrt{2 c_{p,g} T_{in} \left(1 - \left(\frac{p_{aft}}{p_{bef}} \right)^{\frac{\gamma-1}{\gamma}} \right)}} \tag{3.65}$$

All variables in equations (3.59)-(3.65) are explained in Table 3.4. Signals like the angular velocity for the turbine (ω_t), the pressures before and after the turbine (p_{bef} and p_{aft}) and the mass flow through the turbine ($\dot{m}_{turb}$) could be modeled as well. However, these signals are already modeled with a good accuracy in the vehicles ECM and therefore those signals are used as inputs.

Table 3.4: *Nomenclature for the turbocharger model.*

Notation	Description	Unit
A_{sa}	Total area between solid and ambient	$[m^2]$
A_{sg}	Total area between solid and exhaust gas	$[m^2]$
$c_{p,sol}$	Specific heat capacity for the solid (body housing)	$[\frac{J}{kgK}]$
$c_{p,g}$	Specific heat capacity for exhaust gas	$[\frac{J}{kgK}]$
η_t	Efficiency of the turbin	$[-]$
γ	Heat capacity ratio	$[-]$
h_{sa}	Heat transfer coefficient between solid and ambient	$[\frac{W}{m^2K}]$
h_{sg}	Heat transfer coefficient between solid and exh. gas	$[\frac{W}{m^2K}]$
k_0	Tuning parameter for max. turbine efficiency	$[-]$
k_1	Tuning parameter for optimal BSR	$[-]$
m_g	Mass of exhaust gas	$[kg]$
m_{sol}	Mass of solid (body housing)	$[kg]$
$\dot{m}_exh$	Exhaust gas mass flow	$[kg/s]$
$\dot{m}_{turb}$	Exhaust mass flow through turbine	$[kg/s]$
ω_t	Angular velocity of the turbine	$[rad/s]$
p_{aft}	Pressure after turbine	$[Pa]$
p_{bef}	Pressure before turbine	$[Pa]$
$\dot{W}$	Work extracted by turbine	$[W]$
r_t	Radius of turbine	$[m]$
T_{amb}	Temperature of ambient air	$[K]$
T_g	Temperature of exhaust gas exiting turbocharger	$[K]$
T_{in}	Temperature of exhaust gas entering turbocharger	$[K]$
T_{sol}	Temperature of body housing	$[K]$

3.5 Catalyst

A one dimensional approach for the TWC is described in [22]. The authors derive a volume based energy balance, which inspires the approach taken in this study. The energy balance for a control volume in the catalyst is shown in Figure 3.10. Where $\dot{H}_{in}$ represents the enthalpy entering the system as hot exhaust gas. The cylinder labelled "gas phase" represents a control volume of the exchange energies for the gas which flows into the catalyst monolith. The term $\dot{Q}_{cond,gas}$ represents the energy transfer by conduction along the gas phase. The term $\dot{Q}_{conv,gas}$ represents the convective heat transfer in the axial direction. The term $\dot{Q}_{conv,exch}$ represents the convective heat exchange between the solid phase and the gas phase. Which can go both ways since the catalyst brick is heated by the exothermic reactions.

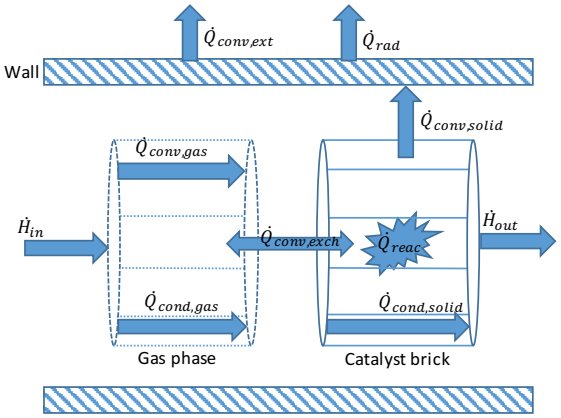

Figure 3.10: *Diagram about the energy balance for the TWC.*

However, some simplifications are made from the energy balance in Figure 3.10. The conduction along the gas phase is neglected since its influence is minor according to [7]. The radiation from the wall is neglected since [16] shows that the influence is not big, but also because the inclusion would require an extra state for the wall temperature. The heat convection to the ambient is also simplified and calculated from the monolith instead of a wall temperature that would require that extra state. Furthermore, the conduction along the substrate should be negligible for cordierite monoliths. However the first monolith in the catalytic converter used in this thesis consists of metal and therefore the term for the thermal conduction is kept in the energy balance. The simplified energy balance is shown in Figure 3.11.

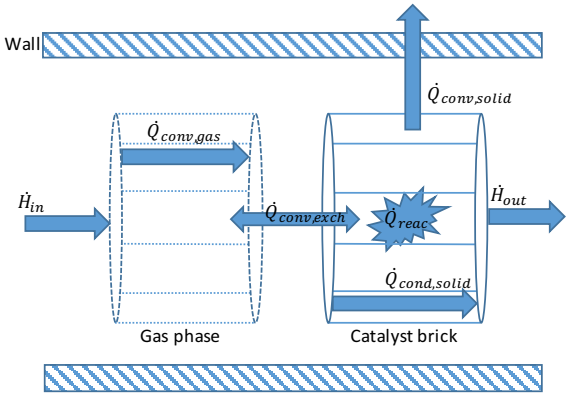

Figure 3.11: *Diagram about the simplified the energy balance for the TWC.*

The PDE for the gas phase is given by

$$c_{p,g} m_g \frac{\partial T_g}{\partial t} = h_{sg} A_{sg} (T_{sol} - T_g) - \dot{m}_{exh} c_{p,g} b \frac{\partial T_g}{\partial z} \tag{3.66}$$

where z is the axial position. The first term on the right hand side accounts for the exchange between the gas and the monolith. The second term on the right hand side accounts for the convective heat transfer along the gas. The corresponding energy balance for the solid phase is given by

$$\begin{aligned} m_{sol} c_{p,sol} \frac{\partial T_{sol}}{\partial t} = k_s A_{cross} b \frac{\partial^2 T_{sol}}{\partial z^2} - h_{sg} A_{sg} (T_{sol} - T_g) \\ - h_{sa} A_{sa} (T_{sol} - T_{amb}) + \sum_i (\Delta H_i R_i) \end{aligned} \tag{3.67}$$

where the first term on the right hand side describes the heat conduction along the substrate, the second term the convective heat transport between the gas and the monolith, the third term describes the heat exchange between the solid and ambient. The last term accounts for the heat released by the exothermic reactions, where the term R_i is the reaction rate and ΔH_i is the reaction enthalpy difference. The estimation of the release enthalpy is straight forward to calculate by chemical balance. However the reaction rate R_i for each reaction is very complex and time consuming to calculate, since this would require kinetic reaction models as well as its own set of PDE to calculate. This is because the concentration of each chemical composition would have to be known, which would result in the model not being suitable for online calculations. Therefore a lumped term suggested in [22] is used, the simplified model is given by

$$\dot{Q}_{reac} = \sum_i (\Delta H_i R_i) = K_{reac} \dot{m}_{exh} \eta_{cat} (T_{sol}) \tag{3.68}$$

where the term K_{reac} is a tunable constant. The authors in [22] have chosen to describe the catalyst efficiency η_{cat} as a hyperbolic function of temperature described by

$$\eta (T_{sol}) = 0.5 \tanh \left(s \left(T_{sol} - T_{light-off} \right) \right) + 0.5 \tag{3.69}$$

where s is the slope of the function and $T_{light-off}$ is the light-off temperature of the catalyst. As seen in (3.68) the reaction energy is assumed to be proportional to the exhaust gas mass flow and catalyst efficiency. Which according to [22] is only a valid assumption when the engine is working under stoichiometric conditions.

To make the model suitable for online use the PDEs has to be discretized both over time and over the axial position. Since the dynamics of the gas are much faster than the dynamics of the solid, the gas temperature T_g can be approximated to be in steady state, which means that the left hand side in (3.66) are set to zero. However, the model in (3.66) still needs to be discretized in the axial direction, which is done by using finite forward difference method. To use finite difference the catalyst is divided into N segments. The discretized model for the gas phase

is given by

$$T_g^{(k)} = \frac{h_{sg}\frac{A_{sg}}{N}T_{sol}^{(k)} + T_g^{(k-1)}\dot{m}_{exh}c_{p,g}}{\dot{m}_{exh}c_{p,g} + h_{sg}\frac{A_{sg}}{N}} \tag{3.70}$$

where k represents a specific segment number and $1 \leq k \leq N$, where N is the number of segments. In addition to this, the left hand side in (3.67) is discretized using the Euler forward method since it requires less resources for computation compared to other methods. Furthermore, the equation also consists of a second order PDE which is discretized by the central difference method. This results in the model being explained by

$$T_{sol}^{(k)}(i) = T_{sol}^{(k)}(i-1) + T_s\frac{dT_{sol}^{(k)}(i-1)}{dt} \tag{3.71}$$

where T_s is the sample time and i is the current sample. The derivative for the solid phase is given by

$$\begin{aligned}\frac{dT_{sol}^{(k)}(i)}{dt} = \frac{k_s A_{cross}}{\frac{m_{sol}}{N}c_{p,sol}}\frac{T_{sol}^{(k+1)} - 2T_{sol}^{(k)} + T_{sol}^{(k-1)}}{\frac{L}{N}} - \frac{h_{sg}\frac{A_{sg}}{N}}{\frac{m_{sol}}{N}c_{p,sol}}\left(T_{sol}^{(k)} - T_g^{(k)}\right) \\ - \frac{h_{sa}\frac{A_{sa}}{N}}{\frac{m_{sol}}{N}c_{p,sol}}\left(T_{sol}^{(k)} - T_{amb}\right) - \frac{\dot{Q}_{reac}}{\frac{m_{sol}}{N}c_{p,sol}}\end{aligned} \tag{3.72}$$

where h_{sg}, h_{sa}, s and K_{reac} are tuning parameters. As mentioned earlier the lumped reaction model in (3.68) is primarily working when the engine is ran in stoichiometric conditions. To make the model applicable on a wider range of lambda values K_{reac} is implemented as an look-up table where the constant K_{reac} varies with different values of λ. Further the heat transfer coefficient for the heat transfer between the exhaust gas and the catalyst brick, h_{sg} depends on exhaust gas mass flow. Therefore this parameter is also implemented as a look-up table, where h_{sg} depends on $\dot{m}_{exh}$. The same thing applies for the heat transfer coefficient between the catalyst and the ambient air, which depends on the vehicle velocity. Therefore h_{amb} is implemented as a look-up table that depends on the vehicle speed. All the parameters from (3.66)-(3.72) are described in Table 3.5.

Table 3.5: *Nomenclature for catalyst models.*

Notation	Description	Unit
A_{cross}	Monolith cross sectional area	$[m^2]$
A_{sg}	Area between solid and gas	$[m^2]$
A_{sa}	Area between solid and ambient	$[m^2]$
b	Thickness of a segment	$[m]$
$c_{p,g}$	Specific heat capacity for exhaust gas	$[J/(kgK)]$
$c_{p,sol}$	Specific heat capacity for the solid	$[J/(kgK)]$
Δh_i	Reaction enthalpy difference	$[J/mol]$
η	Catalyst efficiency	$[-]$
h_{sa}	Heat transfer coefficient between gas and ambient	$[W/(m^2K)]$
h_{sg}	Heat transfer coefficient between gas and solid	$[W/(m^2K)]$
i	Current sample	$[-]$
k	Element number	$[-]$
k_g	Thermal conductivity for exhasut gas	$[W/(mk)]$
k_s	Thermal conductivity for the monolith	$[W/(mk)]$
K_{reac}	Scaling factor for $\dot{Q}_{reac}$	$[-]$
L	Length of catalyst brick	$[m]$
$\dot{m}_{exh}$	Exhaust gas mass flow	$[kg/s]$
m_g	Mass of exhaust gas	$[kg]$
m_{sol}	Mass of the the monolith	$[kg]$
N	Number of elements of the catalyst	$[-]$
$\dot{Q}_{reac}$	Lumped term for the reaction energy	$[W]$
R_i	Reaction rate for the exothermic reactions	$[mol/s]$
s	Slope of the efficiency function	$[-]$
T_{amb}	Ambient temperature	$[K]$
T_g	Temperature of the gas in the catalyst	$[K]$
$T_{light-off}$	Light-off temperature of the catalyst	$[K]$
T_s	Sample time	$[s]$
T_{sol}	Catalyst temperature of the solid	$[K]$

3.6 Downpipe

The purpose of this pipe is to absorb vibrations from the engine and it is connected directly to the catalyst outlet. The energy balance for the pipe is shown in Figure 3.12, where the enthalpy entering and exiting the pipe are denoted $\dot{H}_{in}$ respectively $\dot{H}_{out}$. The convective heat transfer between the exhaust gas and the wall is denoted $\dot{Q}_{conv,gas}$. Since the wall consists of metal, heat will transfer along the pipe which is denoted $\dot{Q}_{cond,wall}$. Further the wall will lose energy to the ambient by convection and radiation, these are denoted $\dot{Q}_{conv,ext}$ and $\dot{Q}_{rad}$ in the figure.

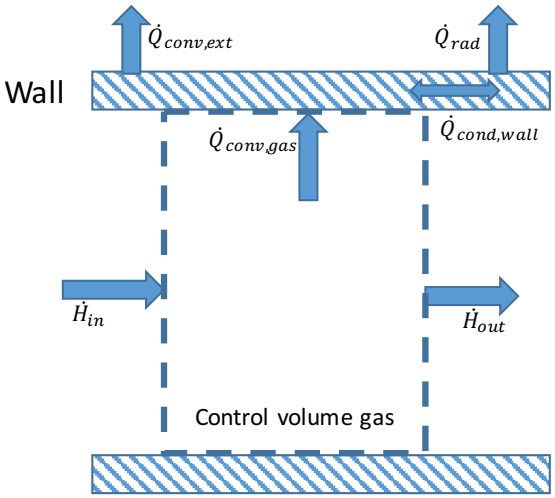

Figure 3.12: *Diagram about the energy balance for the downpipe.*

The energy balance in Figure 3.12 is described by two different states as for the turbocharger. The state for the gas temperature is described by

$$m_g c_{p,g} \frac{dT_g}{dt} = \dot{m}_{exh} c_{p,g} b \frac{\partial T_g}{\partial z} + h_{sg} A_{sg} (T_g - T_w) \tag{3.73}$$

where z is the axial position. The first term on the right hand side accounts for the convection along the pipe and the second term describes the heat exchange between the exhaust gas and the wall. The wall temperature T_w is given by the following equation

$$\begin{aligned} m_w c_{p,w} \frac{dT_w}{dt} = k_s A_{cross} b \frac{\partial^2 T_w}{\partial z^2} + h_{sg} A_{sg} (T_g - T_w) + h_{sa} A_{sa} (T_{amb} - T_w) + \\ \sigma \epsilon A_{sa} (T_{amb}^4 - T_w^4) \end{aligned} \tag{3.74}$$

where the first term on the right hand side accounts for the conduction along the material, the second term describes the heat exchange between the gas and the wall. The third term accounts for the convective heat transfer to the ambient and the last term describes the energy lost by radiation to the ambient.

As mentioned in Section 3.5, PDEs like these has to be discretetized to be applicable for the ECM. Since the dynamics of the exhaust gas are much faster than for the wall temperature, T_g can be approximated to be in steady state. The first term in (3.73) is discretized in the axial direction by applying the forward difference method. This results in T_g being described by

$$T_g^k(i) = \frac{\dot{m}_{exh} c_{p,g} T_g^{k-1}(i) + h_{sg} \frac{A_{sg}}{N} T_w^k(i)}{\dot{m}_{exh} c_{p,g} + h_{sg} \frac{A_{sg}}{N}} \tag{3.75}$$

where k is the current segmet, i is the current sample and N the total amount of segments. Furthermore, Eq. (3.74) is discretized both over time and the axial direction. The time derivative is solved by applying the Euler forward method which gives the wall temperature

$$T_w(i) = T_w(i-1) + T_s \frac{dT_w(i-1)}{dt} \tag{3.76}$$

where the derivative in (3.74) is discretized over the axial position by applying the central diffference method since the equation consists of a second order PDE, this gives

$$\frac{dT_w^k(i)}{dt} = \frac{1}{\frac{m_w}{N} c_{p,w}} \Bigg[k_s A_{cross} \frac{T_w^{k+1}(i) - 2T_w^k(i) + T_w^{k+1}(i)}{\frac{L}{N}} + h_{sg} \frac{A_{sg}}{N} \left(T_g^k(i) - T_w^k(i) \right) + h_{sa} \frac{A_{sa}}{N} \left(T_{amb}^k(i) - T_w^k(i) \right) + \sigma \epsilon \frac{A_{sa}}{N} \left(T_{amb}^{4^k}(i) - T_w^{4^k}(i) \right) \Bigg] \tag{3.77}$$

All parameters from (3.73)-(3.77) are described in Table 3.6.

Table 3.6: *Nomenclature for the downpipe.*

Notation	Description	Unit
A_{sa}	Total area between wall and ambient	$[m^2]$
A_{sg}	Total area between wall and exhaust gas	$[m^2]$
b	Thickness of one segment	$[m]$
$c_{p,g}$	Specific heat capacity for exhaust gas	$[\frac{J}{kgK}]$
$c_{p,w}$	Specific heat capacity for the wall	$[\frac{J}{kgK}]$
ϵ	Emissivity of wall	$[-]$
h_{sa}	Heat transfer coefficient between wall and ambient	$[\frac{W}{m^2K}]$
h_{sg}	Heat transfer coefficient between wall and exh. gas	$[\frac{W}{m^2K}]$
i	Current sample	$[-]$
k	Current segment	$[-]$
L	Length of pipe	$[m]$
m_g	Mass of exhaust gas	$[kg]$
$\dot{m}_{exh}$	Exhaust gas mass flow	$[kg/s]$
m_w	Mass of pipe wall	$[kg]$
N	Number of segments	$[N]$
σ	Stefan–Boltzmann's constant	$[\frac{W}{m^2K^4}]$
T_{amb}	Temperature of ambient air	$[K]$
T_g	Temperature of exhaust gas	$[K]$
T_w	Wall temperature	$[K]$

4

Results and Discussion

This chapter contains the obtained results from the modeling and includes a discussion about the results.

4.1 Measurement Data

The models are parameterized and validated on different data sets. The same data is used for estimation and validation of the catalyst and the downpipe model. Another data set is used for the turbo model since pressure sensors before and after the turbine did not work during the first two measurement sessions. Figures 4.1-4.3 represent the estimation data that is used. The following Figures 4.4-4.8 represent the validation data that is used.

4.1.1 Estimation Data

The different estimation data sets will be described under this section.

Turbocharger

The turbocharger is parameterized with an ambient temperature around $293°K$. The mass flow, lambda value, engine speed and the engine torque during the measurements used for the parametrization of the turbocharger model are shown in Figure 4.1. Furthermore, the vehicle speed, ambient temperature, temperature before turbine and the temperature after the turbine for this measurement are shown in Figure 4.2.

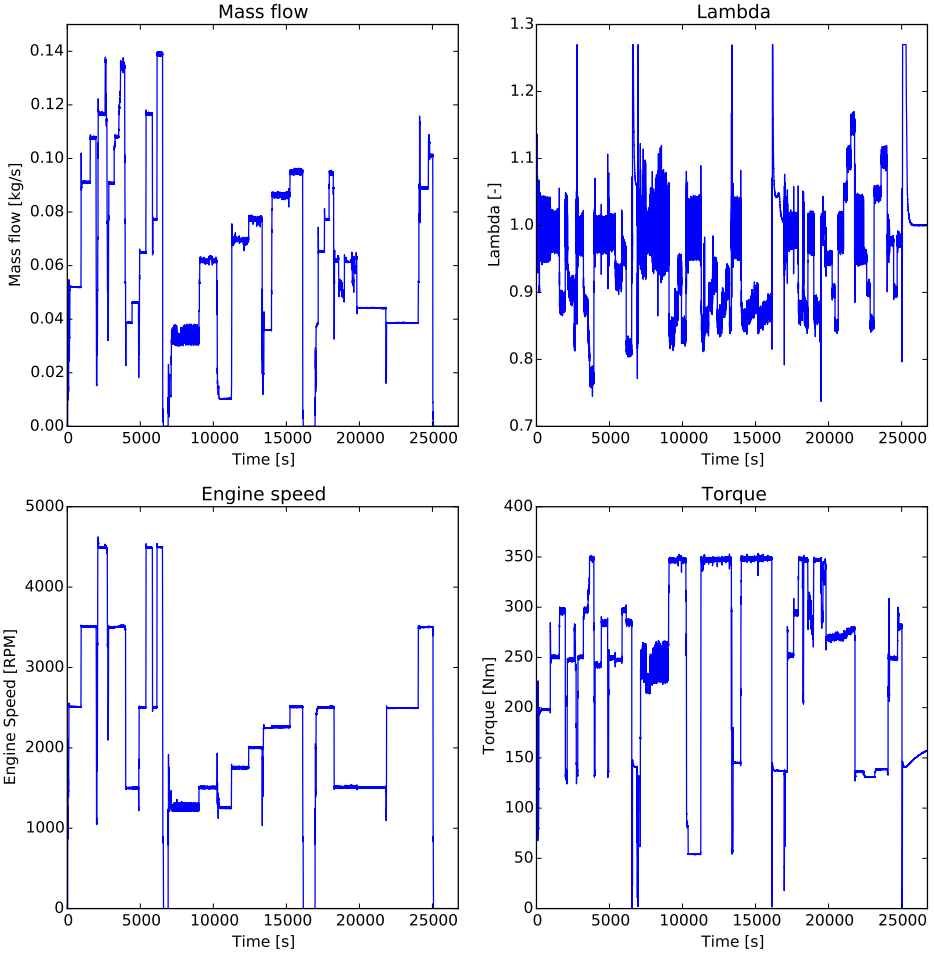

Figure 4.1: *Plots of the mass flow, lambda value, engine speed and the engine torque during the measurements used for parameterization of the turbocharger model.*

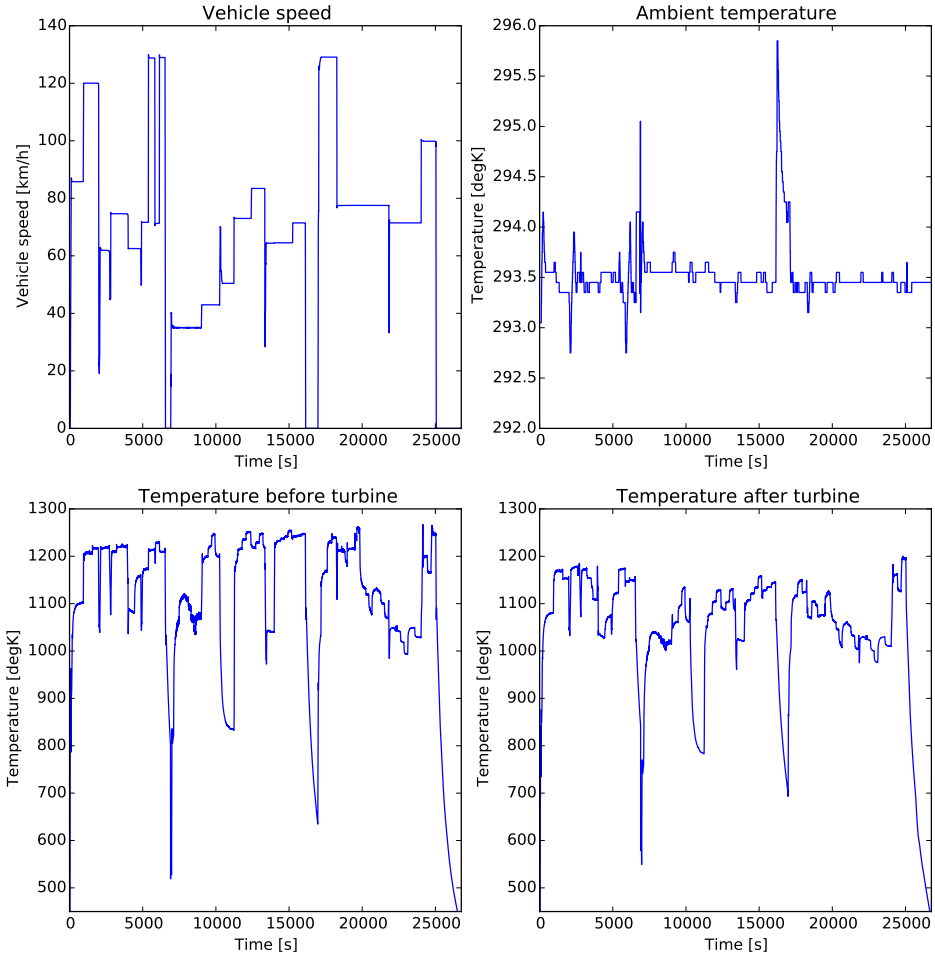

Figure 4.2: *Plots of vehicle speed, ambient temperature and temperatures before and after the turbine during the parameterization of the turbocharger model.*

Catalyst and Downpipe

The catalyst model and the downpipe models are parameterized with two different ambient temperatures and several load and vehicle speed steps. The exhaust gas mass flow, lambda value, engine speed and the torque during the measurements for the parameterization for the catalyst and downpipe models are shown in Figure 4.3. The vehicle speed and the ambient temperature are shown in Figure 4.4. The temperature before the first catalyst brick, which is used as input signal for the catalyst model and the temperature 25 mm into the first brick, which is used as output signal from the model are also shown in Figure 4.4. Furthermore, the temperature before and after the downpipe which are used as input

and output signals for the downpipe model are also shown in Figure 4.4.

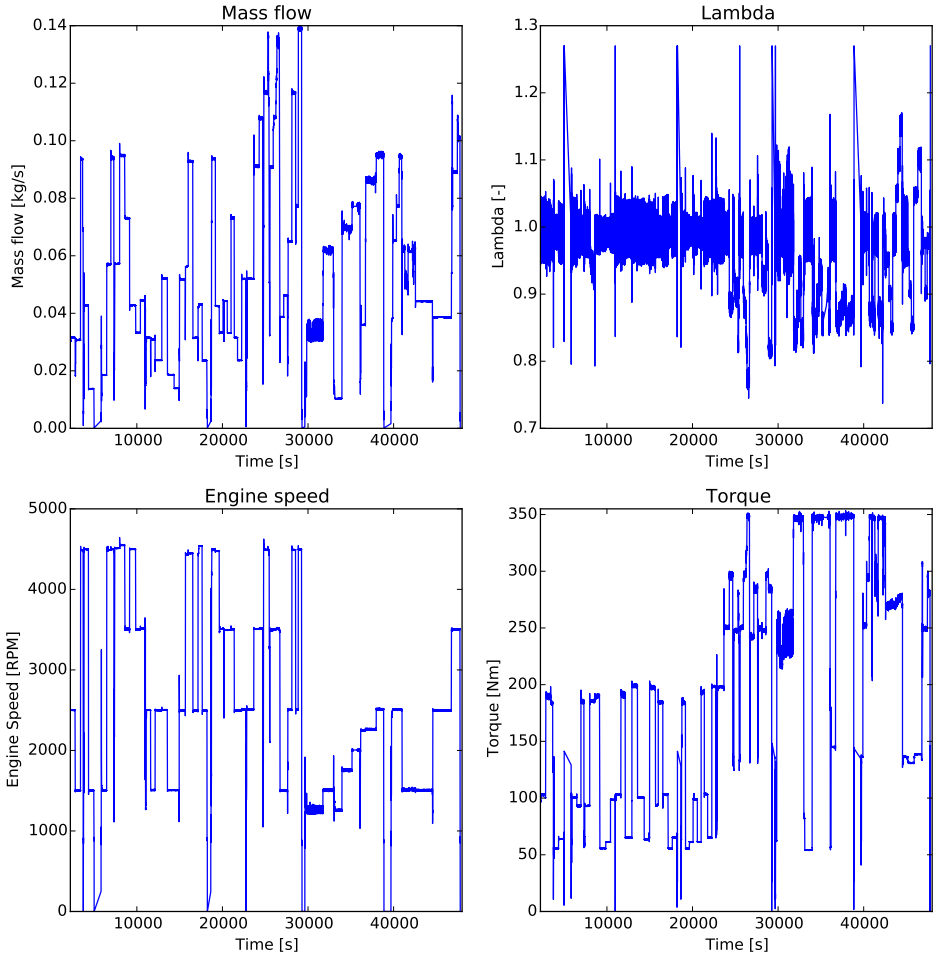

Figure 4.3: *Plots of the mass flow, lambda value, engine speed and the engine torque during the parameterization of the catalyst and downpipe models.*

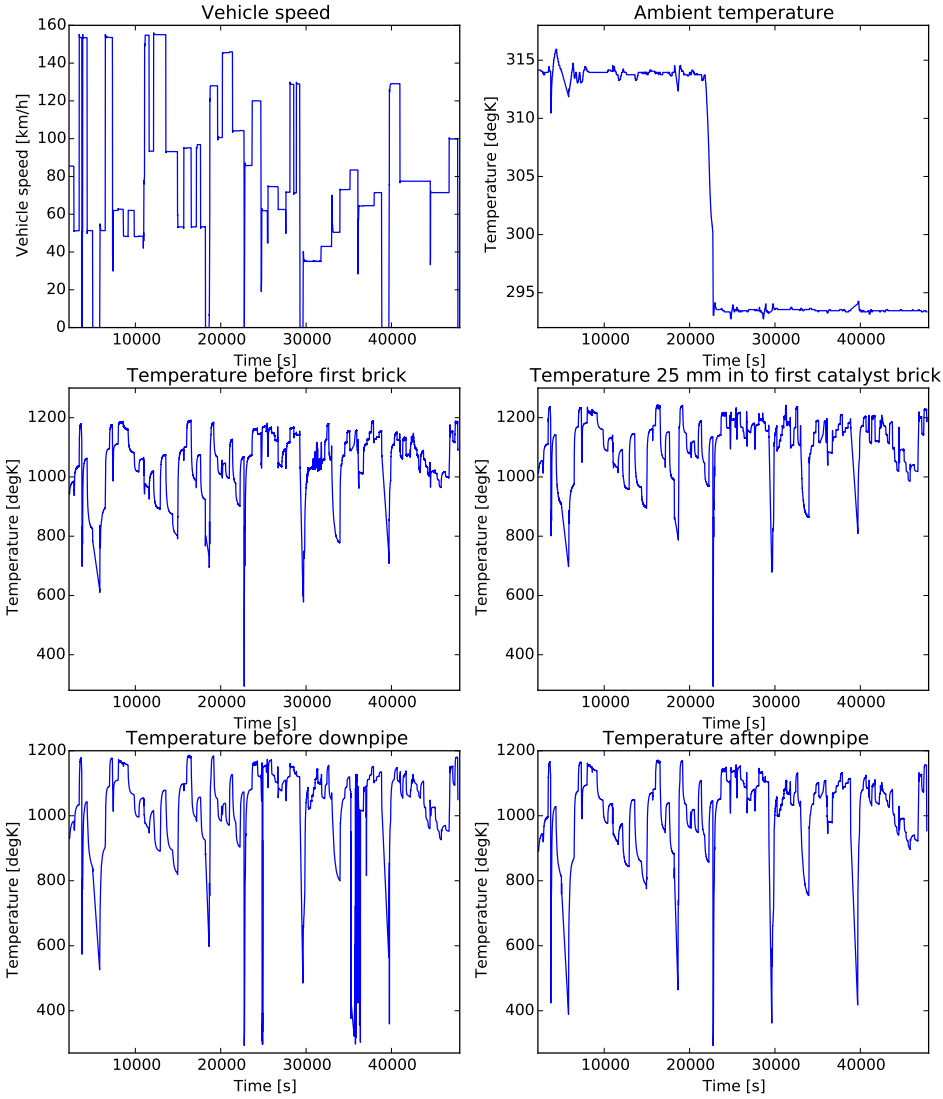

Figure 4.4: *Plots of vehicle speed, ambient temperature, temperature before the first catalyst brick, temperature 25 mm in to the first catalyst brick, temperature before downpipe and the temperature after the downpipe during the parameterization of the catalyst and downpipe models.*

4.1.2 Validation Data

The different validation data sets will be described under this section.

Turbocharger

The driving scenario for the validation data for the turbocharger is shown in Figure 4.5. The figure shows the exhaust gas mass flow, the lambda value, the engine speed and the engine torque during the measurements used for the validation data. The vehicle speed and the ambient temperature together with the temperature before and after the turbine for the same data set are shown in Figure 4.6. The temperature before the turbine is used as input signal to the turbocharger model and the temperature after the turbine is used for comparison against the modeled output.

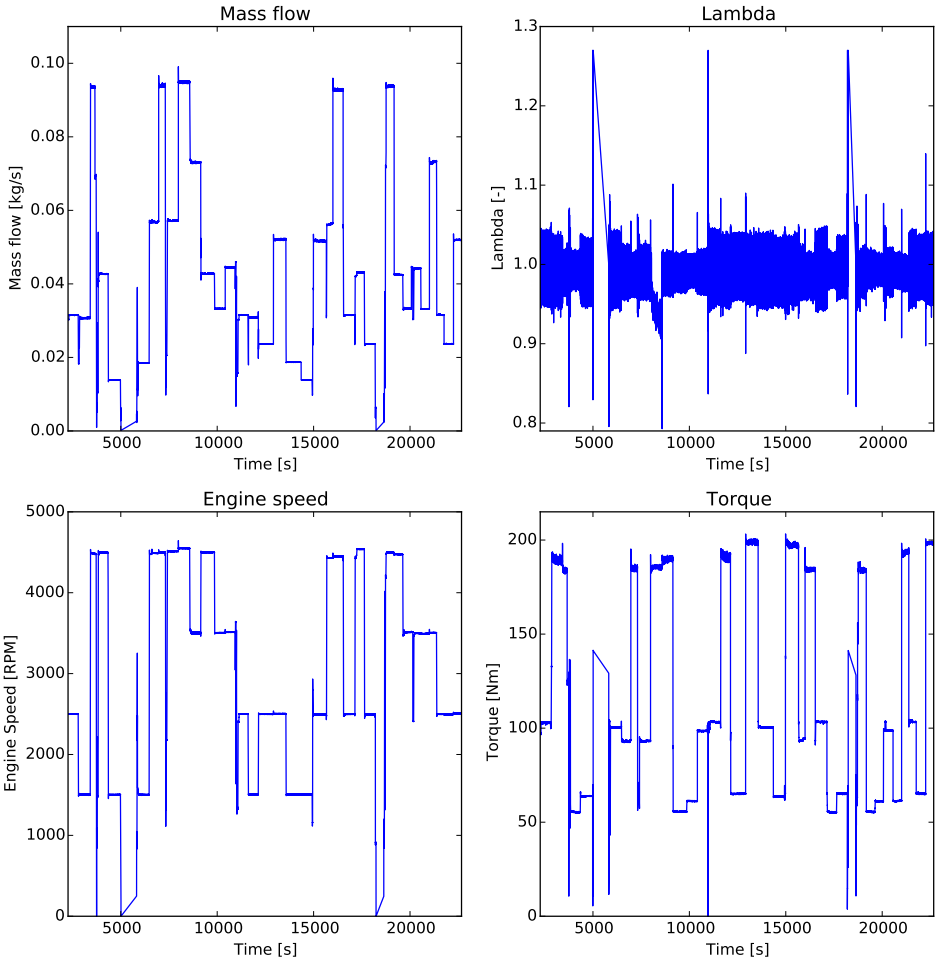

Figure 4.5: *Plots of the mass flow, lambda value, engine speed and the engine torque during the validation of the turbocharger model.*

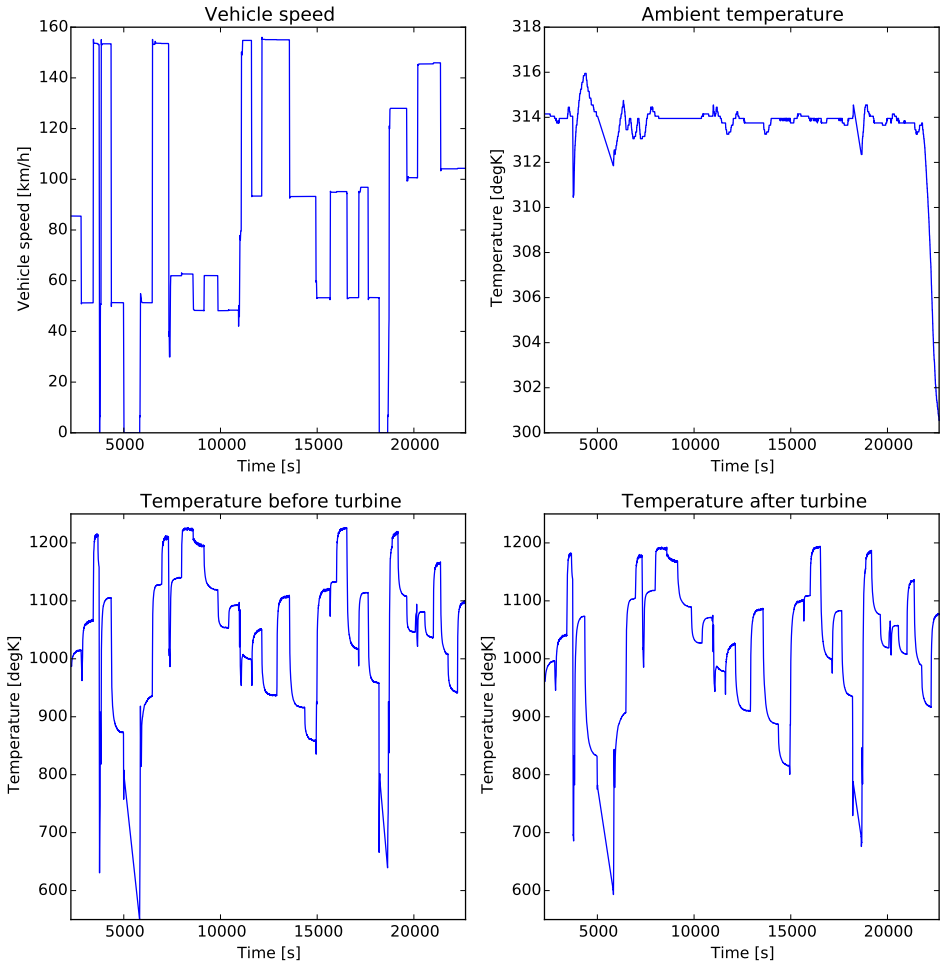

Figure 4.6: *Plots of vehicle speed, ambient temperature and temperatures before and after the turbine during the validation of the turbocharger model.*

Catalyst and Downpipe

Figure 4.7 shows the exhaust gas mass flow, lambda value, engine speed and the engine torque during the measurement for the validation data for the catalyst and the downpipe model. Furthermore the vehicle speed, ambient temperature, temperature before the first catalyst brick, temperature 25 mm in to the first catalyst brick and the temperature before and after the downpipe during the measurements for the validation of the catalyst and the downpipe are shown in Figure 4.8.

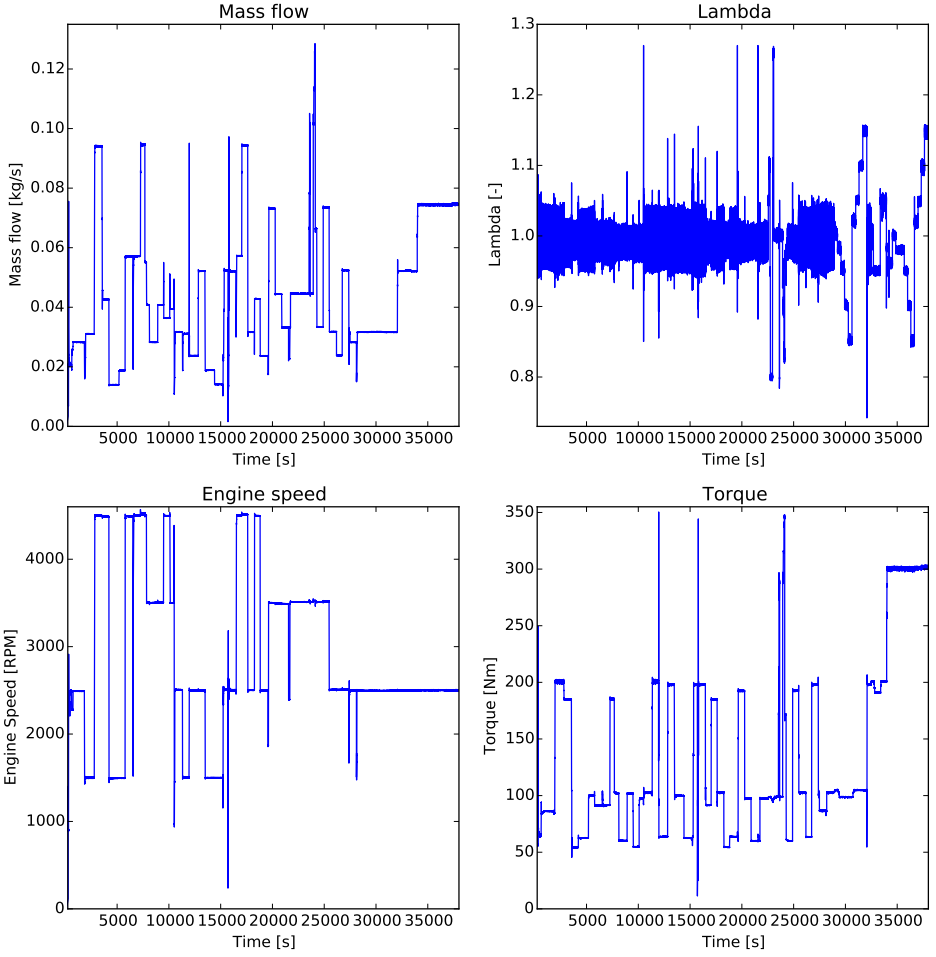

Figure 4.7: *Plots of the mass flow, lambda value, engine speed and the engine torque during the validation of the catalyst and downpipe models.*

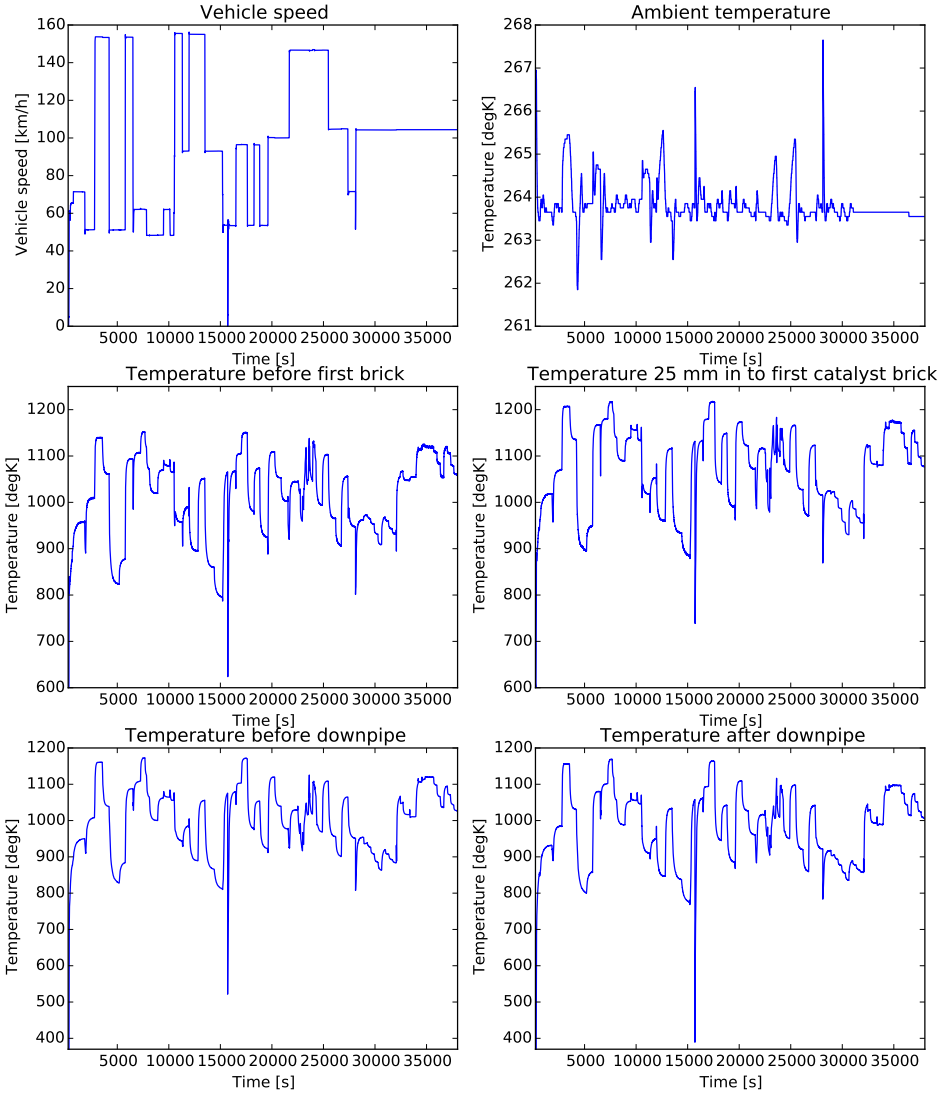

Figure 4.8: *Plots of vehicle speed, ambient temperature, temperature before the first catalyst brick, temperature 25 mm in to the first catalyst brick, temperature before downpipe and the temperature after the downpipe during the validation of the catalyst and downpipe models.*

4.2 Model Accuracy

All validated models will be presented with a mean absolute percentage error MAPE which looks as follows

$$e = \frac{1}{n} \sum_{k=1}^{n} \left| \frac{m_k - \hat{m}_k}{m_k} \right| \cdot 100 \tag{4.1}$$

where m_k is the measured signal, $\hat{m}_k$ is the modeled signal and n the total amount of samples. The represented residuals in the results is obtained from the measurements and the model by following

$$y_{res} = y_{mod} - y_{meas} \tag{4.2}$$

4.3 Cylinder-Out Temperature

Models for the cylinder-out temperature have been derived where the models are based on several submodels that represent different parts of the Otto cycle. In the models some assumptions are made in order to reduce the model complexity. In some cases multiple submodels are proposed so different options are available.

A challenge that may occur when implementing the cylinder-out temperature model is to have the right sampling rate. The right sampling rate will in this case be crank angle based. This may be tricky since all signals have to be converted to this domain. Another challenge that will arise is validation of the combustion process which is fast and vary from cycle to cycle. In order to get better understanding of the in-cylinder processes and to more easily validate the models it would be valuable to measure cylinder pressure. It would also be of value to measure the engine block temperature at different locations around the cylinder and especially around exhaust port. This should be done to get a deeper understanding of the heat transfer in these areas.

Other simplifications that have been made is that the crevices are not included in the in-cylinder model. The reason for this is since a first approach of a simple model is needed. When this model is implemented and validated, future work can consist of expanding the in-cylinder model with a crevice model.

4.4 Exhaust Manifold

As described in section 3.3 a problem occurs due to the pulsations in the exhaust manifold. The mass of the thermocouple situated closer to the turbocharger gets more affected by pulsations and that is why the artificial signal may be needed. A good result was not achieved due to time limitations and simplifications. Firstly it is hard to construct a pulsating signal from an averaged measured signal. There were simply not enough information to construct a realistic signal. The constructed signal was made as a square wave since this was the easiest way. An alternative would be to shape the constructed signal with smoother edges as in Figure 3.6, so it gets more of a sinusoidal shape.

From the measurements performed it is clear that it is colder closer to the engine block which acts as a heat sink which agrees with the observations made in [9]. This is due to the fact that the coolant cools the engine block, thus conduction is present along the pipes towards the engine block.

As assumed before measuring it is possible to see from the measurements that different parts of the exhaust manifold have different temperatures. One reason for this is that one does not have the same bulk flow all over the surface which leads to different convective heat coefficients towards the surroundings.

4.5 Turbocharger

The measured signals that are used for this model are the pressure and temperature before and after the turbine. The rest of the signals are obtained from the control system of the vehicle. The measured pressures are used instead of the modeled pressure signals from the ECM since the signal for the pressure after the turbine was forgotten to be saved during the measurement. The absolute mean percentage error MAPE for the turbo model is 0.46 %. The parameterization is first made on estimation data and then the model is compared to saved validation data. Figure 4.9 shows the measured temperature together with the modeled temperature after the turbine.

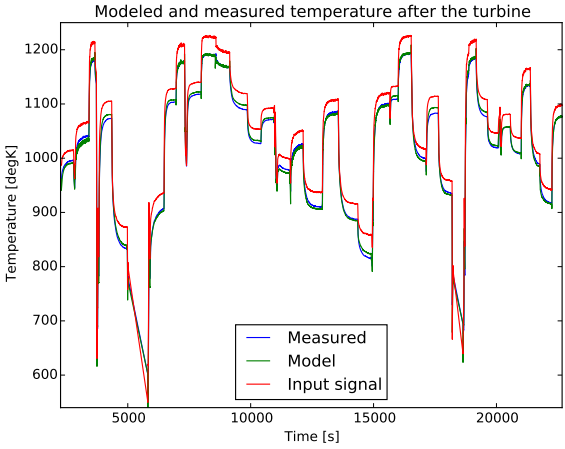

Figure 4.9: *Plot of the measured and the modeled temperature after the turbine. For the different load steps, engine speeds steps and vehicle speed steps in Figure 4.5 and 4.6.*

Furthermore Figure 4.10 shows the error between the measured and the modeled temperature. The error is presented as a residual as well as in a histogram. The residual is obtained from (4.2).

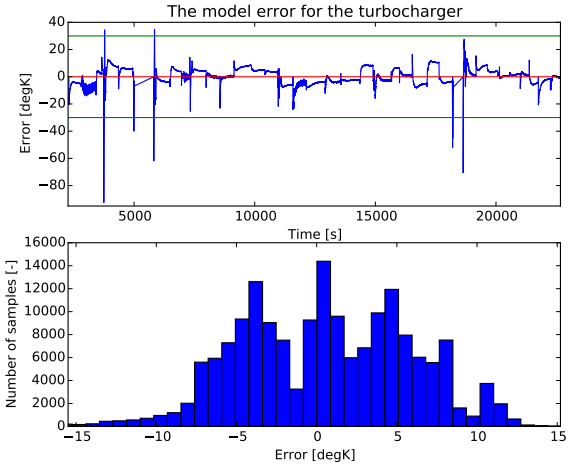

Figure 4.10: *Residual and a histogram of the error from the simulation in Figure 4.9, where the residual is calculated by subtracting the measured temperature from the modeled temperature. The larger three deviations in the residual are initial transients that occurs due to measurement file changes, since multiple measurement sessions are joint together for this simulation. The horizontal green lines are set to values of -30 and 30.*

The modeled efficiency is shown in Figure 4.11. Both heat transfer coefficients are implemented as look-up tables for this model. The optimized heat transfer coefficients are shown in Figure 4.12.

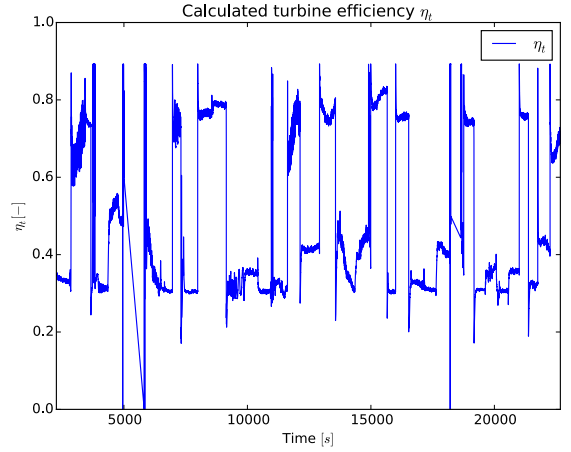

Figure 4.11: *The modeled turbine efficiency η_t.*

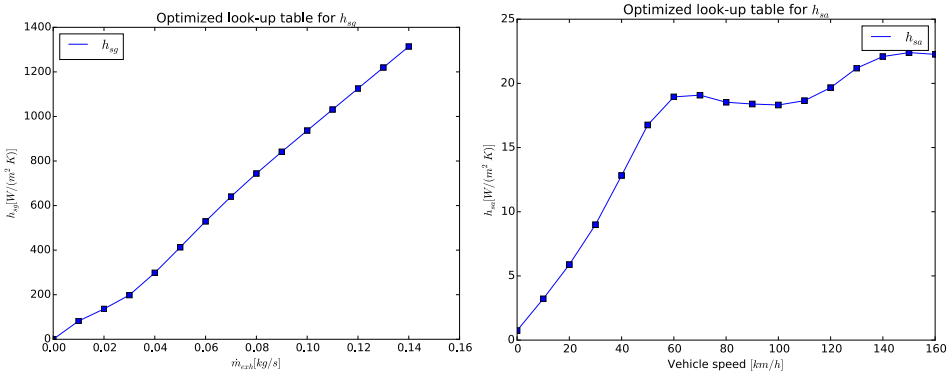

(a) *(b)*

Figure 4.12: *Plots of the optimized look-up tables for the heat transfer coefficient. Where* ***(a)*** *shows the table for* h_{sg} *and* ***(b)*** *the table for* h_{sa}*.*

The values of the optimized parameters for the model are presented in Table 4.1. Only the specific heat capacities are kept constant, the rest of the parameters are optimized. The look-up table for the specific heat capacity for the exhaust gas used in this model is presented in Table 4.2.

Table 4.1: *Presents the optimized parameters for the results.*

Parameter	Value	Unit
A_{sg}	0.035	m^2
A_{sa}	0.08	m^2
$C_{p,solid}$	600	$J/(kgK)$
γ	1.39	–
k_0	0.89	–
k_1	1.14	–
m_{solid}	0.68	kg
T_s	0.1	s

The suggested model should be able to perform even better if the wall temperature is measured as well, since this will allow the wall state to be optimized towards measurement data. Furthermore, all optimized parameters have obtained physical values. However, unrealistic values are obtained for the maximal efficiency which can be seen in Figure 4.11. The efficiency reaches values up to around 0.9. This is too high in comparison to the turbine map which gives a maximum efficiency around 0.7.

Table 4.2: *The optimized look-up table for the specific heat coefficient for the exhaust gas. The specific heat capacity for the exhaust gas is approximated to be the same as for air.*

$T[K]$	$c_{p,air}\left[\frac{J}{kgK}\right]$
280	1006
300	1007
350	1009
400	1014
450	1021
500	1030
600	1051
800	1099
1000	1141
1200	1175
1400	1207

4.6 Catalyst

The temperatures that are modeled in the results are measured 25 and 50 mm into the first brick. The model is divided into 15 segments, since this gives a brick thickness of 4 mm which gives a relatively good fit for both the first temperature sensor (25 mm in to the first brick) and the second sensor that is measuring the temperature 50 mm in to the first brick. The 15 bricks division means that the temperature for the 7:th brick is modeled approximately 25 mm into the first brick whereas the 13:th brick models the temperature exactly 50 mm into the first brick.

As mentioned in Section 2.2.1 cool down experiments are performed. For the catalyst these measurements are used to parameterize the heat transfer coefficient between the catalyst brick and the ambient air (h_{sa}). The simulation and model fitting are shown in Figure 4.13. Notice that the model only fits the measurement during the cool down, since h_{sa} is the only parameter that is parameterized when the engine is turned off the python code is rewritten to make the simulation possible. The code is modified since the model does not handle unrealistic cases such as in Figure 4.13 where the engine is turned off but the vehicle is still running on high speeds. However, the model is still the same throughout this section. Figure 4.13 shows that the model is initiated on the measured temperature right before the cool down starts. The optimized look-up table for the heat transfer coefficient to the surroundings, h_{sa} is shown in Figure 4.14. The parameterized look-up table is kept constant for the parameterization performed on the rest of the parameterization data. For this model the look-up tables h_{sa}, h_{sg} and K_{reac} are the tunable parameters, where h_{sa} is only parameterized with the cool-down measurements. In addition to these tuning parameters some fixed parameters are used in the catalyst temperature model. A look-up table for the thermal con-

ductivity is shown in Table 4.3. The values in the table are obtained from a data sheet for the specific material used in the first catalyst brick.

The specific heat capacity for the first catalyst brick is also implemented as a look-up table where the source for the data is the same as for the thermal conductivity. Furthermore, the specific heat capacity for the exhaust gas is approximated to be the same as air. The look-up data used for this is shown in Table 4.2. The rest of the non-tunable parameters that are used in the catalyst model are presented in Table 4.4.

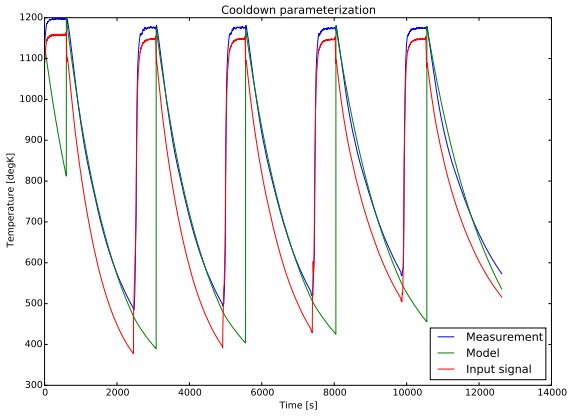

Figure 4.13: *Plot of the optimized simulation of the cool down experiment. The temperature is modeled and measured 25 mm into the first brick. The vehicle speed in the first cool down is performed at a speed of* 160 *km/h, the second at a speed of* 120 *km/h following by* 80 *km/h,* 40 *km/h and* 0 *km/h. The ambient temperature is kept at a constant temperature of* $-10°C$*. The* MAPE *is* 1.14 *% for the cool down part of this simulation.*

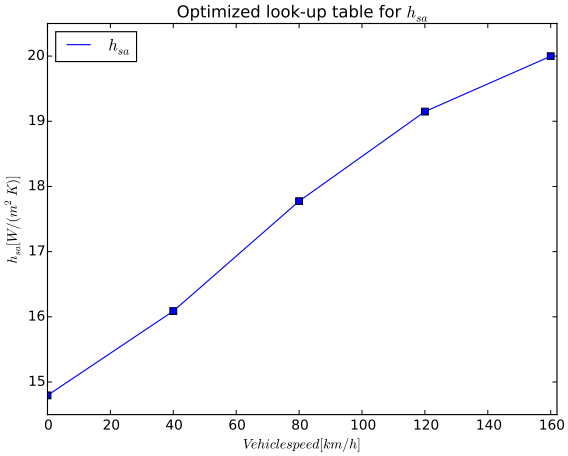

Figure 4.14: *The optimized look-up table for the heat transfer coefficient between the first catalyst brick and the surroundings.*

Furthermore, the modeled catalyst temperature 25 mm into the first brick together with the measured value for a 10 hour drive is shown in Figure 4.15. The corresponding temperature 50 mm in to the first catalyst brick is shown in Figure 4.16. The residual and histogram showing the difference between the modeled value and the measured value is shown in Figure 4.17 and 4.18. Furthermore the MAPE is 1.01% for the temperature 25 mm into the first brick and 2.07 % for the temperature 50 mm into the first brick.

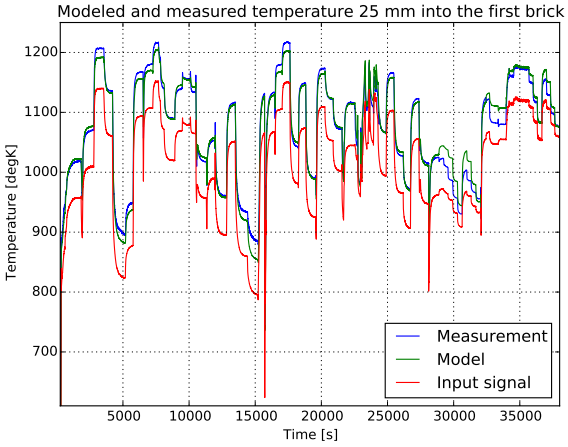

Figure 4.15: *The measured catalyst temperature together with the modeled temperature 25 mm into the first catalyst brick.*

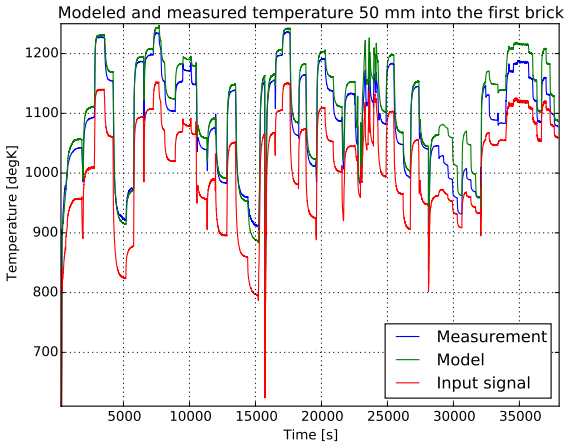

Figure 4.16: *The measured catalyst temperature together with the modeled temperature 50 mm into the first catalyst brick.*

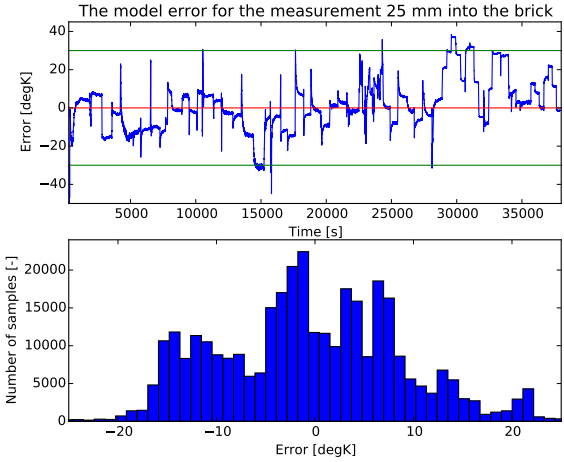

Figure 4.17: *The residual and a histogram of the error from the simulation in Figure 4.15, where the residual is calculated by subtracting the measured temperature from the modeled temperature.*

The optimized look-up table for the reaction constant is shown in Figure 4.19b. The Figure shows that the reaction constant is highest around lambda $\bar{1}$ which agrees with the physics, that says that exothermic reactions are largest when the engine runs in stoichiometric conditions. Further, the optimized heat transfer coefficient between the gas phase and the solid phase is shown in Figure 4.19a.

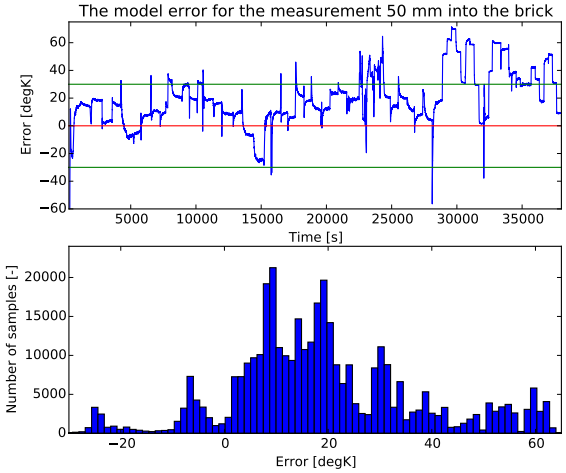

Figure 4.18: *The residual and a histogram of the error from the simulation in Figure 4.16, where the residual is calculated by subtracting the measured temperature from the modeled temperature.*

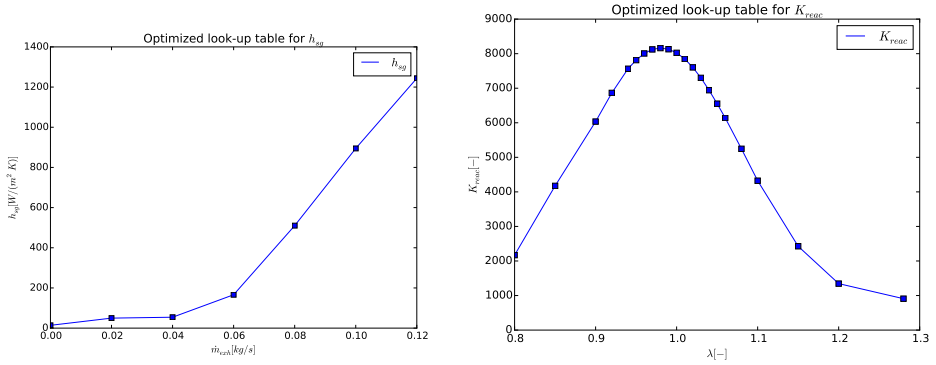

(a) ***(b)***

Figure 4.19: *Plots of the optimized look-up tables for the heat transfer coefficient between gas phase and the solid phase as well as the optimized look-up table for the reaction constant. Where* ***(a)*** *shows the table for h_{sg} and* ***(b)*** *the table for K_{reac}.*

Table 4.3: *Each value of the obtained look-up table for the thermal conductivity for the first catalyst brick.*

$T[K]$	373	473	573	673	773	873	973	1073	1173
$k_{cat}\left[\frac{W}{mK}\right]$	10.9	12.4	13.9	15.5	16.9	18.2	19.7	21.1	22.5

Table 4.4: *Values of the non tunable parameters.*

Parameter	Value	Unit
A_{cross}	0.0024	m^2
A_{sg}	2.71	m^2
A_{sa}	0.0233	m^2
b	0.004	m
L	0.06	m
m_s	0.915	kg
s	0.01	–
$T_{light-off}$	553	K
T_s	0.1	s

The results show that the model is working fairly well. However in Figure 4.15 and 4.17 in between 30000-35000 seconds the error is fairly large. The reason for this is that between those times the lambda value is manually controlled to be somewhere between 0.8 and 1.2. This shows that the model is not as good when lambda departs from being around one for longer time periods. This is most probably because of the lumped term simplifications for the reactions. The issue could not be solved with a look-up table for the reaction term with lambda as input. As future work it is suggested to test the model with a 2D look-up table for the reaction coefficient with lambda and the exhaust gas mass flow as input signals, instead of a value that is proportional to the mass flow. In case that does not give results that are good enough, a kinetic model for the reactions should be investigated more thoroughly.

Furthermore, all of the optimized parameters have obtained realistic values. The catalyst temperature could be more precise if the wall temperature for the catalyst is included in the model as a state. This was not tested in this thesis due to lack of time.

4.7 Downpipe

To acquire the results presented in this section the exhaust temperature is measured in the beginning and in the end of the pipe, also the wall temperature in the end of the pipe. The model is also divided into 10 segments to be able to describe the thermal conduction along the pipe. The amount of segments is a trade of between accuracy and model complexity. The modeled temperature together with the measured temperature is shown in Figure 4.20. The MAPE for this simulation is 1.07 %.

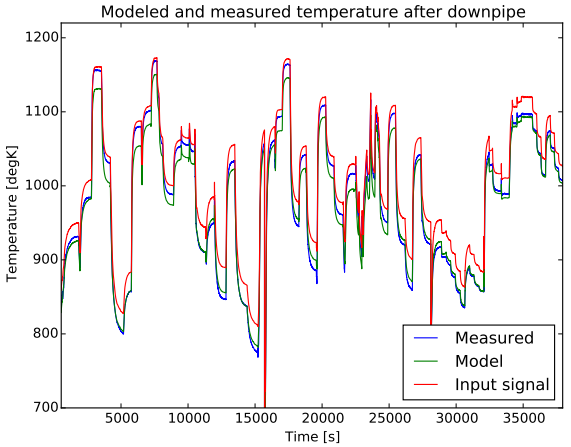

Figure 4.20: *Measured and the modeled temperature after the downpipe.*

Furthermore Figure 4.21 shows the error between the measured and the modeled temperature. The error is presented as a residual as well as in a histogram. The large peak in the residual exists because of initial transients due to a file change.

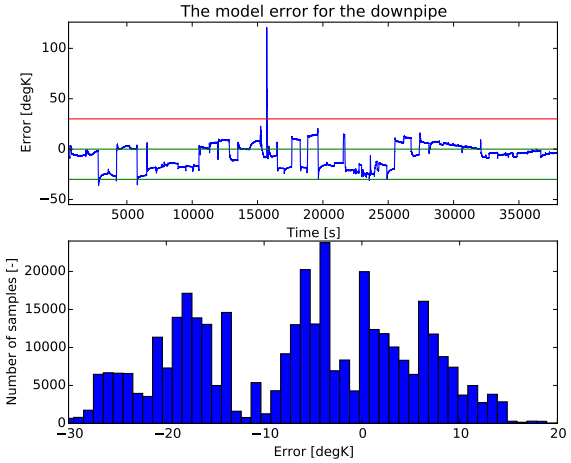

Figure 4.21: *Residual and a histogram of the error from the simulation in Figure 4.20, where the residual is calculated by subtracting the measured temperature from the modeled temperature.*

Both heat transfer coefficients are implemented as look-up tables for this model as well. The optimized heat transfer coefficients are shown in Figure 4.22.

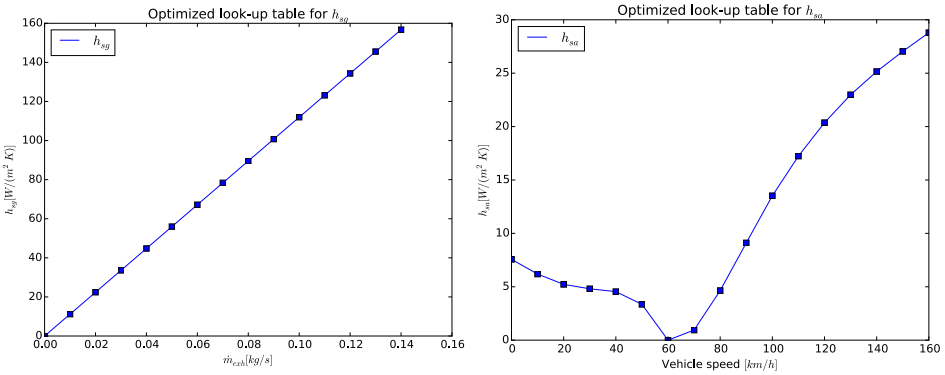

(a) *(b)*

Figure 4.22: *Plots of the optimized look-up tables for the heat transfer coefficient. Where* ***(a)*** *shows the table for* h_{sg} *and* ***(b)*** *the table for* h_{sa}*.*

Furthermore, the look-up table used for $c_{p,g}$ is presented in Table 4.2. The tuneable parameters for this model are the look-up tables for h_{sa} and h_{sg}, and the parameters A_{sa}, k_s and ϵ. The rest of the parameters are constant and are shown in Table 4.5.

Table 4.5: *Presents the optimized parameters for the results.*

Parameter	Value	Unit
A_{cross}	0.00096	m^2
A_{sa}	0.12	m^2
A_{sg}	0.09	m^2
$C_{p,w}$	500	$J/(kgK)$
ϵ	0.5	–
k_s	694.8	$\frac{W}{mK}$
m_w	0.63	kg
N	10	kg
σ	$5.67 \cdot 10^{-8}$	$\frac{W}{m^2K^4}$
T_s	0.1	s

The results shows that the suggested model is working fine. However maybe one would expect even better results since it basically is a pipe that is modeled. One reason for the model not being perfect could be that the thermal conduction along the pipe is not consistent due to the flexible part which consists of a different material. The optimized parameters have obtained good values, except for the two points being close to zero in the look-up table for the heat transfer coefficient between the wall and the ambient, shown in Figure 4.22b. This most probably happens because there are not enough measurement points at that vehicle speed,

as seen in Figure 4.4. This results in a bad interpolation for those values and therefore it is suggested to use less data points in the look-up table. Another suggestion to make the model even better is to divide the pipe in to two different parts. Where the parameters are different for the flexible part and for the solid part, which is left for future work.

5

Conclusions and Future Work

This thesis has contributed to a deeper understanding of physical modeling of the exhaust system. By extensive measurements it has been possible to study the thermal behavior of the exhaust system, starting from the exhaust manifold all the way until the downpipe. The measurements have given information about how the temperature vary in different parts in the exhaust system. This project has also given deeper understanding of how measurements should be performed. From measurements it has also been seen that one have to tackle measurements error since they are impossible to avoid.

Throughout this thesis three different models have been developed and validated for the turbocharger, the catalyst and the downpipe. Two theoretical models have been developed. One for the temperature out from the cylinder and one for the temperature drop over the exhaust manifold. The validated models have decreased the model complexity compared to the map-based models and the overall agreement with measurement data is good.

The turbocharger model that has been developed in this thesis has a model error that lays in between -10 and 10 degrees. In some few regions the error of the model exceeds these values. The model has an MAPE of 0.46 %.

The catalyst model that is developed in this thesis gives an error that mostly lies in between -20 and 20 degrees. The developed catalyst model includes a simplified reaction term which does not give as accurate model values when lambda is not held close to 1 for longer periods. The model has an MAPE of 1.01 %.

The downpipe model that is developed throughout this thesis give an MAPE of 1.07 %. The error from this model lays mostly in between -30 and 20 degrees. In order to improve the model it can be tried to extend the model into multiple

submodels.

Concerning the exhaust manifold model a hypothesis is done when it comes to the exhaust pulsation in the system. The increase in temperature over the exhaust manifold is therefore considered as a pulsating problem. Due to this the exhaust model could not be completely validated.

5.1 Future Work

As future work, the engine out temperature model and the exhaust manifold model should be validated. Concerning the catalyst model it would be interesting to implement the reaction term as a 2D map with both mass flow and lambda value as input signals. If that does not give results accurate enough, a kinetic model for the exothermic reactions in the catalyst should be investigated further. To improve the results for the turbocharger the temperature of the body housing should be measured, this to be able to parameterize the wall temperature against measurement data. The conductive heat transfer to the compressor side should also be investigated more thoroughly. As mentioned in the results the downpipe can be improved by splitting the pipe into two different parts. Where the parameters are different for the flexible part and for the solid part. Further, all models need to be implemented into the ECM of the vehicle.

Bibliography

[1] Habib Aghaali and Hans-Erik Angstrom. Temperature estimation of turbocharger working fluids and walls under different engine loads and heat transfer conditions. In *SAE Technical Paper*. SAE International, 09 2013. doi: 10.4271/2013-24-0123. URL http://dx.doi.org/10.4271/2013-24-0123. Cited on page 3.

[2] Filip Ainouz and Jonas Vedholm. Mean value model of the gas temperature at the exhaust valve. Master's thesis, Linköping University, SE-581 83 Linköping, 2009. Cited on page 3.

[3] Ingemar Andersson. Cylinder pressure and ionization current modeling for spark ignited engines. Technical report, isy, 2002. LiU-TEK-LIC-2002:35, Thesis No. 962. Cited on page 3.

[4] Stanislav V. Bohac, Douglas M. Baker, and Dennis N. Assanis. A global model for steady state and transient s.i. engine heat transfer studies. In *SAE Technical Paper*. SAE International, 02 1996. doi: 10.4271/960073. URL http://dx.doi.org/10.4271/960073. Cited on page 3.

[5] D. Bresch-Pietri, T. Leroy, and N. Petit. Control-oriented time-varying input-delayed temperature model for si engine exhaust catalyst. In *American Control Conference (ACC), 2013*, pages 2189–2195, June 2013. doi: 10.1109/ACC.2013.6580160. Cited on page 4.

[6] J.A. Caton and J.B. Heywood. Models for heat transfer, mixing and hydrocarbon oxidation in a exhaust port of a spark-ignited engine. In *SAE Technical Paper*. SAE International, 02 1980. doi: 10.4271/800290. URL http://dx.doi.org/10.4271/800290. Cited on page 3.

[7] Christopher Depcik and Dennis Assanis. One-dimensional automotive catalyst modeling. *Progress in Energy and Combustion Science*, 31(4):308 – 369, 2005. ISSN 0360-1285. doi: http://dx.doi.org/10.1016/j.pecs.2005.08.001. URL http://www.sciencedirect.com/science/article/pii/S0360128505000237. Cited on page 38.

[8] Lars Eriksson. *Spark Advance Modeling and Control*. PhD thesis, Linköpings Universitet, May 1999. Cited on page 2.

[9] Lars Eriksson. Mean value models for exhaust system temperatures. In *SAE Technical Paper*. SAE International, 03 2002. doi: 10.4271/2002-01-0374. URL http://dx.doi.org/10.4271/2002-01-0374. Cited on pages 3, 28, 29, 30, and 55.

[10] Lars Eriksson and Ingemar Andersson. An analytic model for cylinder pressure in a four stroke si engine. In *SAE Technical Paper*. SAE International, 03 2002. doi: 10.4271/2002-01-0371. URL http://dx.doi.org/10.4271/2002-01-0371. Cited on pages 2, 3, and 21.

[11] J. A. Gatowski, E. N. Balles, K. M. Chun, F. E. Nelson, J. A. Ekchian, and John B. Heywood. Heat release analysis of engine pressure data. In *SAE Technical Paper*. SAE International, 10 1984. doi: 10.4271/841359. URL http://dx.doi.org/10.4271/841359. Cited on page 24.

[12] Lee Kyu Hyun, Shim Chang Yeul, and Kim Wan-Bum. Development of dual wall air gap exhaust system. In *SAE Technical Paper*. SAE International, 03 2000. doi: 10.4271/2000-01-0205. URL http://dx.doi.org/10.4271/2000-01-0205. Cited on page 3.

[13] Farzad Keynejad and Chris Manzie. Cold start modelling of spark ignition engines. *Control Engineering Practice*, 19(8):912 – 925, 2011. ISSN 0967-0661. doi: http://dx.doi.org/10.1016/j.conengprac.2011.05.005. URL http://www.sciencedirect.com/science/article/pii/S0967066111001079. Cited on page 3.

[14] Lars Nielsen Lars Eriksson. *Modeling and Control of Engine and Drivelines*. Wiley, 2014. ISBN 978-1-118-47999-5. Cited on pages 3, 4, 18, 21, 22, 23, 25, 26, and 36.

[15] Michael Mladek and Christopher H. Onder. A model for the estimation of inducted air mass and the residual gas fraction using cylinder pressure measurements. In *SAE Technical Paper*. SAE International, 03 2000. doi: 10.4271/2000-01-0958. URL http://dx.doi.org/10.4271/2000-01-0958. Cited on pages 3 and 19.

[16] G. Montenegro and A. Onorati. 1d thermo-fluid dynamic modeling of reacting flows inside three-way catalytic converters. *SAE Int. J. Engines*, 2: 1444–1459, 04 2009. doi: 10.4271/2009-01-1510. URL http://dx.doi.org/10.4271/2009-01-1510. Cited on page 38.

[17] Paul Moraal and Ilya Kolmanovsky. Turbocharger modeling for automotive control applications. In *SAE Technical Paper*. SAE International, 03 1999. doi: 10.4271/1999-01-0908. URL http://dx.doi.org/10.4271/1999-01-0908. Cited on page 4.

[18] Mohit Hashemzadeh Nayeri. Cylinder-by-cylinder torque model of an si-

engine for real-time applications. Master's thesis, Linköping University, SE-581 83 Linköping, 2005. Cited on page 3.

[19] Hee Jun Park. *Development of an in-cylinder heat transfer model with variable density effects on thermal boundary layers*. PhD thesis, The university of the Michigan, 2009. URL http://deepblue.lib.umich.edu/bitstream/handle/2027.42/62428/heej?sequence=1. Cited on page 3.

[20] S. Koteswara Rao, Rayees Imam, Karthik Ramanathan, and S. Pushpavanam. Sensitivity analysis and kinetic parameter estimation in a three way catalytic converter. *Industrial & Engineering Chemistry Research*, 48(8):3779–3790, 2009. doi: 10.1021/ie801244w. URL http://dx.doi.org/10.1021/ie801244w. Cited on page 4.

[21] Alessandro Romagnoli and Ricardo Martinez-Botas. Heat transfer analysis in a turbocharger turbine: An experimental and computational evaluation. *Applied Thermal Engineering*, 38:58 – 77, 2012. ISSN 1359-4311. doi: http://dx.doi.org/10.1016/j.applthermaleng.2011.12.022. URL http://www.sciencedirect.com/science/article/pii/S1359431111007198. Cited on page 3.

[22] Stefano Sabatini, Irfan Kil, Joseph Dekar, Travis Hamilton, Jeff Wuttke, Michael A Smith, Mark A Hoffman, and Simona Onori. A new semi-empirical temperature model for the three way catalytic converter. *IFAC-PapersOnLine*, 48(15):434 – 440, 2015. ISSN 2405-8963. doi: http://dx.doi.org/10.1016/j.ifacol.2015.10.062. URL http://www.sciencedirect.com/science/article/pii/S2405896315019382. 4th {IFAC} Workshop on Engine and Powertrain Control, Simulation and Modeling E-COSM 2015Columbus, Ohio, USA, 23-26 August 2015. Cited on pages 3, 4, 28, 29, 37, and 39.

[23] Daniel W. Wendland. Automobile exhaust-system steady-state heat transfer. In *SAE Technical Paper*. SAE International, 04 1993. doi: 10.4271/931085. URL http://dx.doi.org/10.4271/931085. Cited on page 3.

[24] Fredrik Westin, Jörgen Rosenqvist, and Hans-Erik Ångström. Heat losses from the turbine of a turbocharged si-engine - measurements and simulation. In *SAE Technical Paper*. SAE International, 03 2004. doi: 10.4271/2004-01-0996. URL http://dx.doi.org/10.4271/2004-01-0996. Cited on pages 4 and 34.

[25] Saïd Zidat and Michael Parmentier. Exhaust manifold design to minimize catalyst light-off time. In *SAE Technical Paper*. SAE International, 03 2003. doi: 10.4271/2003-01-0940. URL http://dx.doi.org/10.4271/2003-01-0940. Cited on page 3.

[26] Per Öberg and Lars Eriksson. Control oriented modeling of the gas exchange process in variable cam timing engines. In *SAE Technical Paper*.

SAE International, 04 2006. doi: 10.4271/2006-01-0660. URL http://dx.doi.org/10.4271/2006-01-0660. Cited on pages 3 and 19.